# Variable Speed Wind Turbine Dynamic Model Validation

JWT measurements and simulations

J.T.G. Pierik (ECN) J. Morren (TUD)

#### ABSTRACT

In this report the Variable Speed Pitch (VSP) wind turbine dynamic model, developed by ECN and TUD in the Erao-2 project, is validated. Simulation results are compared to measurements of the JWT variable speed wind turbine in Sweden. Two types of measurements have been used: measurements during normal operation and a voltage dip. For the first set of measurements, the Auto Power Spectral Density functions (APSDs) of measurement and simulation are compared. For the voltage dip, the time series of power and reactive power are compared. The wind turbine dynamic model calculates instantaneous voltages and currents and includes the dynamics of the doubly fed indiction generator and its control but does not include the switching process of the power electronic converter. This is an argument for elimination of the high frequency noise on the measurements, for instance by calculating RMS or moving average values. Results with and without averaging are compared.

A complicating factor in this validation of the VSP model was the limited amount of information that was available for the JWT turbine, basically only the parameters in a commercial brochure. This is only a fraction of the parameters required by the dynamic turbine model. To bypass this severe problem, the parameters of a similar VSP-DFIG were used in the validation. For this alternative turbine a complete and consistent set of parameters was available. Not knowing the parameters of the measured turbine, severely limits the validation results. A better set of variable speed turbine measurements was not available however, neither in the IEA Annex XXI data base nor at ECN-TUD.

The results for normal operation and voltage dip deviated on a number of points from the measurements, as could be expected. The deviations were sometimes relatively small and never extremely large. Within the limitation caused by the unavailability of turbine parameters, the validation results seem to be acceptable.

This report is the third of a set of three reports that documents the results of the project "Verificatie dynamische modellen van windparken (Erao-3)" and the K-Project "Validatie van windparkmodellen voor netstudies". The other two reports are entitled:

- Validation of dynamic models of wind farms (Erao-3): Executive summay, benchmark results and model improvements [6];
- Constant Speed Wind Farm Dynamic Model Validation: Alsvik measurements and simulations [5].

**Keywords:** wind turbine models, wind farm models, model validation, wind farm dynamics, wind farm electrical systems

# Acknowledgement

Erao-3 is a continuation of the Erao projects on the development of steady state (load flow) and economic models (Erao-1) and dynamic models of offshore wind farms (Erao-2). The Erao projects have been supported by the Dutch Agency for Energy and Environment (NOVEM) in the "Programma Duurzame Energie" of the Netherlands, executed by Novem by order of the Ministry of Economic Affairs.

The measurement data of the JWT wind turbine have been supplied by Chalmers University of Technology in the framework of the IEA Annex XXI: Dynamic models of Wind Farms for Power System studies.

Novem project number: 2020-02-12-10-002 ECN project numbers: 7.4336 and 7.9463

Variable Speed Wind Turbine Dynamic Model Validation

# **CONTENTS**

1	Intro	oduction	7
2	VSP	model validation method	8
	2.1	Using the measured voltage as input	9
3	JWI	T turbine and turbine data	11
	3.1	Turbine parameters	11
4	VSP	wind turbine model	12
5	JWT	VSP-DFIG wind turbine model validation	17
	5.1	Normal operation	17
	5.2	Full power measurement	18
	5.3	Full power simulation	
	5.4	Comparing full power measurement and simulation results	24
	5.5	Half power measurement	28
	5.6	Half power simulation	
	5.7	Comparing half power measurement and simulation results	
	5.8	Low power measurement	37
	5.9	Low power simulation	38
	5.10	Comparing low power measurement and simulation results	42
		Symmetrical voltage dip measurement	
	5.12	Voltage dip simulation	49
6	Con	clusions and recommendations	52
	6.1	Discussion of the validation results	52
	6.2	Conclusion	53
	6.3	Recommendation	53
A	Mod	el improvement	56
В	Calc	ulation of positive sequence, fundamental harmonic and RMS values	57
	B.1	Steady-state conditions	57
	B.2	Non steady-state conditions	58
C	Simi	ılation parameters	62

ECN-E-07-008 5

Variable Speed Wind Turbine Dynamic Model Validation			
•			

#### 1 INTRODUCTION

ECN and TUD have developed steady state and dynamic models of wind turbines and wind farms in the Erao-1 and Erao-2 project [4, 7, 8]. These models can be used to investigate the dynamic behavior of grid connected wind turbines and wind farms and to improve wind turbine control, wind farm control and grid control. The wind turbine and wind farm models, in combination with (partial) grid models, can be also be used to study voltage and frequency transients, small signal stability, effect of wind power on rotating reserve, grid response during short circuits and other extreme events.

This report is one of three reports that document the results of the Erao-3 project "Electrical and control aspects of Offshore wind farms". The other two reports are titled:

- Validation of dynamic models of wind farms (Erao-3): Executive summary, benchmark results and model improvements [6];
- Constant Speed Stall Wind Farm Dynamic Model Validation: Alsvik measurements and simulations [5];

For the problem definition, objectives, method and overview of the results is referred to the summary report [6].

In this report the Variable Speed Pitch (VSP) wind turbine dynamic model of the Erao-2 project is validated. Simulation results are compared to measurements of the JWT wind turbine in Sweden. Two types of measurements are available: measurements during normal operation and a voltage dip. For the measurements during normal operation the Auto Power Spectral Density functions (APSDs) of measurement and simulation will be compared, since the instantaneous rotor effective wind speed during the measurement is not known. For the voltage dip, the effect of the instantaneous rotor effective wind speed is small and the time series of instantaneous or moving average active and reactive power can be compared.

This validation of the VSP wind turbine dynamic model is part of a joint validation effort in IEA Annex XXI: Dynamic models of Wind Farms for Power System studies. Information on Annex XXI can be found in the summary report [6]. The members of IEA Annex XXI chose the measurements on the JWT turbine for the validation of the VSP wind turbine model. The main reasons are:

- only a few alternative measurements of variable speed turbines were available;
- the alternative measurements presented several drawbacks (experimental instead of commercial turbine, measurement did not meet the requirements, limited information on turbine parameters etc.).

This report describes the validation process in a number of steps:

- the validation method is described in chapter 2;
- chapter 3 and 4 summarize the JWT turbine and the VSP turbine dynamic model;
- the simulation results of the VSP-DFIG model are compared to the measurements in chapter 5;
- chapter 6 discusses the validation results and the limitations encountered in the validation process.

# 2 VSP MODEL VALIDATION METHOD

The dynamic model of the variable speed wind turbine will be validated by comparing simulations of the JWT VSP wind turbine to the JWT measurements. Two types of measurements will be used:

- 1. measurements during normal operation;
- 2. measurement of a symmetrical voltage dip.

Measurements of an asymmetrical (unbalanced) voltage dip were also available, but since the model assumes symmetrical (balanced) conditions, this measurement was not used. The measurements during normal operation can be used to validate the mechanical as well as the electrical part of the model, including the wind input model and the power control. The validation can cover a wide range of dynamic phenomena of low as well as high frequency. Which part of the dynamic behavior can be validated, depends on the variables measured, the sample frequency and the duration of the measurement. The measurements of the JWT turbine did not include mechanical variables, however.

The validation for normal operation will compare the frequency response of the model to the frequency content of the measurements, i.e. Auto Power Spectral Density (APSD) values will be compared. In this part of the validation, the emphasis is on the low and medium range frequency content (0.1-100 Hz). Directly comparing time series of individual signals is problematic, as was discussed in [3].

For the relatively fast events during a voltage dip or short circuit, the operational condition of the mechanical part of the turbine, and thus the actual rotor effective wind speed, is less relevant. In that case, time series of measured and simulated variables can be compared directly, conversion to the frequency domain is not required.

The validation process includes the following steps:

- 1. Investigation of the available JWT measurements;
- 2. Preparation of a complete list of input parameters required for the Erao-2 dynamic wind turbine model;
- 3. Preparation of the JWT wind turbine model using the component models in the Erao-2 model library;
- 4. Calculation of the input signals from the measurement: single point average wind speed and generator terminal voltage in dq-reference frame;
- 5. Calculation of a (normalised) rotor effective wind speed time series for the turbine, based on the single point average wind speed in the measurement. The rotor effective wind speed is a statistical realisation for the given rotor diameter and wind regime;
- 6. Execution of the simulation (this may requires a few iteration steps);
- 7. Post processing of simulation and measurement data, preparation of APSDs;
- 8. Evaluation of the results, suggestions for improvements, implementation of improvements, possibly restart from step 6.

#### 2.1 Using the measured voltage as input

In the validation of the Alsvik constant speed wind farm model [3], a problem caused by using the wind turbine terminal voltage as an input for the simulation of normal operation has been discussed. Since the rotor averaged rotationally sampled wind speed in the measurement (i.e. the rotor effective wind speed) is not known (only a single point measurement on a mast near the turbine is given), the rotor effective wind speed in the simulation will not match the measured voltage. Using the measured voltage as an input, therefore results in errors in the calculated APSDs. The error depends on the coherence between the rotor effective wind speed and the voltage. If the coherence is small, the error will also be small. For the Alsvik wind farm it was demonstrated that the coherence between wind speed and the voltage was sufficiently low to permit the use of the measured voltage as input [3]. This is expected to be true for the JWT turbine also, since it is variable speed turbine. A low coherence between the rotor effective wind speed and the terminal voltage of a variable speed turbine is highly probable, due to the decoupling of the wind speed and the active and reactive power by the control of the power electronic converter. Therefore, the VSP model validation will use the measured voltage as an input for the simulations of normal operation. It should be mentioned that not using the measured voltage, while preventing errors caused by the convolution of two input signal which are biased, introduces an error also since the independent part of the voltage variation is not taken into account.

The measured voltage can be used as input in a number of ways:

- 1. as measured, viz. instantaneous three phase voltage values, converted to the dq-reference frame of the model;
- 2. converted to instantaneous positive sequence values, eliminating the zero sequence component, thus producing a symmetrical signal<sup>1</sup>;
- 3. converted to the moving average value (RMS in case of AC phase voltage and current), thus eliminating high frequency components;
- 4. converted to the fundamental harmonic positive sequence moving average value, additionally eliminating low frequency harmonic components.

The choice will depend on the type of model to be verified. For models which assume symmetrical conditions and calculate only fundamental harmonic RMS values, it makes sense to choose the last option, eliminating everything except the first harmonic positive sequence RMS value. For models which calculate instantaneous values, in varying degrees of detail (for example including or excluding the switching of power electronic converters), it makes more sence to use instantaneous measured voltage values or positive sequence moving average values.

The IEA Annex XXI suggested to use the fundamental harmonic positive sequence RMS values of voltage, current and the resulting active power and reactive power for comparison with simulation results [9]. The reasons given for this choice are:

- most power system simulator models only calculate symmetrical conditions but perfectly balanced conditions can not generally be assumed, especially voltage dips are often unbalanced;
- most power system simulator models are phasor-type models, meaning that the voltages and currents are positive sequence RMS values.

<sup>&</sup>lt;sup>1</sup>Appendix B explain different methods of calculating sequence components

The Erao-2 VSP wind turbine model includes an electrical system model based on space phasor theory [1], which calculates instantaneous values under symmetrical conditions. This is different from a phasor-type RMS model in the second argument. Space phasor models are primarily developed for converter control design and evaluations of electrical transients under balanced conditions. Therefore, it is logical to use the instantaneous positive sequence voltage values as input. However, the Erao-2 electrical models do not include the switching of power electronic converters, the IGBT converters are treated as controlled voltage sources. Therefore, the frequency components in the range of the switching frequency (1 kHz) and higher will not be represented correctly for systems with a converter and should be disregarded. An advantage of the use of RMS or fundamental harmonic voltage as input is that the high frequency components are eliminated. On the other hand, the part of the high frequency content, that is not caused by switching of converters, may be represented correctly by the model, but is lost as well. A second disadvantage of the use of RMS or fundamental harmonic values is that extreme values in the voltage and current are reduced. Correct prediction of peak values is an important aspect of models and of model validation. In this report the results from both methods, using instantaneous and moving average RMS values, will be compared for the voltage dip case (see section 5.12). For the normal operation cases instantaneous voltages will be used but only the frequency range 0.1-100 Hz is compared, the high frequency content is disregarded.

# 3 JWT TURBINE AND TURBINE DATA

The JWT turbine is a pitch regulated variable speed turbine based on the doubly fed induction generator concept. The turbine is located in the south of Sweden, about 100 km from the west coast [10]. Table 1 gives the main data of the JWT turbine.



Figure 1: JWT turbine and data acquisition (Chalmers University of Technology)

Table 1: Main data of the JWT

Rated voltage (star)	690 V
Rated power	850 kW
Rotor diameter	52 m
Rotor speed	14-31 rpm
Cut-in wind speed	4 m/s
Nominal wind speed	16 m/s
Maximum wind speed	25 m/s

# 3.1 Turbine parameters

Information on turbine construction, components and control was very limited. The only data available was from a commercial brochure, basically the data in table 1. Since most of the parameters needed for the dynamic model of the JWT variable speed wind turbine with doubly fed induction generator are not available, the parameters of a similar, though bigger, VSP-DFIG turbine have been used (NM92). The alternative turbine is equiped with pitch control, designed by ECN Wind Energy. The control of the DFIG is based on the Internal Model Control (IMC) method and designed by TU Delft [7]. A complete list of the parameters of the VSP wind turbine dynamic model can be found in appendix C.

The unavailability of the JWT parameters is an important drawback in the validation of the VSP wind turbine model. A similar evaluation by Chalmers University of Technology [10], which used the same JWT measurements and the same limited number of turbine data, showed that even with this limitation, a reasonable agreement between measurements and simulations could be achieved. A better variable speed option was not available in Annex XXI (see chapter 1).

# 4 VSP WIND TURBINE MODEL

The VSP wind turbine model validated in this report has been developed by ECN and TUD in the Erao-2 project. The model is programmed in Simulink, a simulation language for dynamic modelling and controller design. The preprocessor, which generates the normalised rotor effective (rotationally sampled) wind speed, is programmed in Matlab. The VSP wind turbine model consists of two main parts:

- the aerodynamic and mechanical system model, including the blade pitch controller and the torque master controller;
- the electrical system model, including the field oriented control of the doubly fed induction generator.

For the general description of the VSP wind turbine dynamic model is referred to [7], available at the web site of ECN (*www.ecn.nl*). The model includes the following components:

- · aerodynamic coefficients module;
- rotor (pitch angle, thrust, torque and azimuth);
- pitch controller;
- drive train (two masses, spring and damper);
- tower (nodding and naying motion of tower top);
- doubly fed induction generator model (space vector fourth order model);
- rotor side converter (controlled voltage source);
- controller of the rotor converter (controls generator torque and stator reactive power);
- DC link;
- grid converter (controlled voltage source);
- controller of the grid side converter (controls DC link voltage and grid side converter reactive power);
- cable between DFIG and transformer;
- three winding transformer;
- voltage source or grid model.

Figures 2 to 6 are a selection of Simulink model diagrams of the VSP-DFIG model. Figure 2 is the main diagram with submodels representing the main components of the turbine and the input signals wind and grid voltage. Figure 3 shows the wind model which calculates the rotor effective wind speed based on a given average wind speed and the position of the rotor.

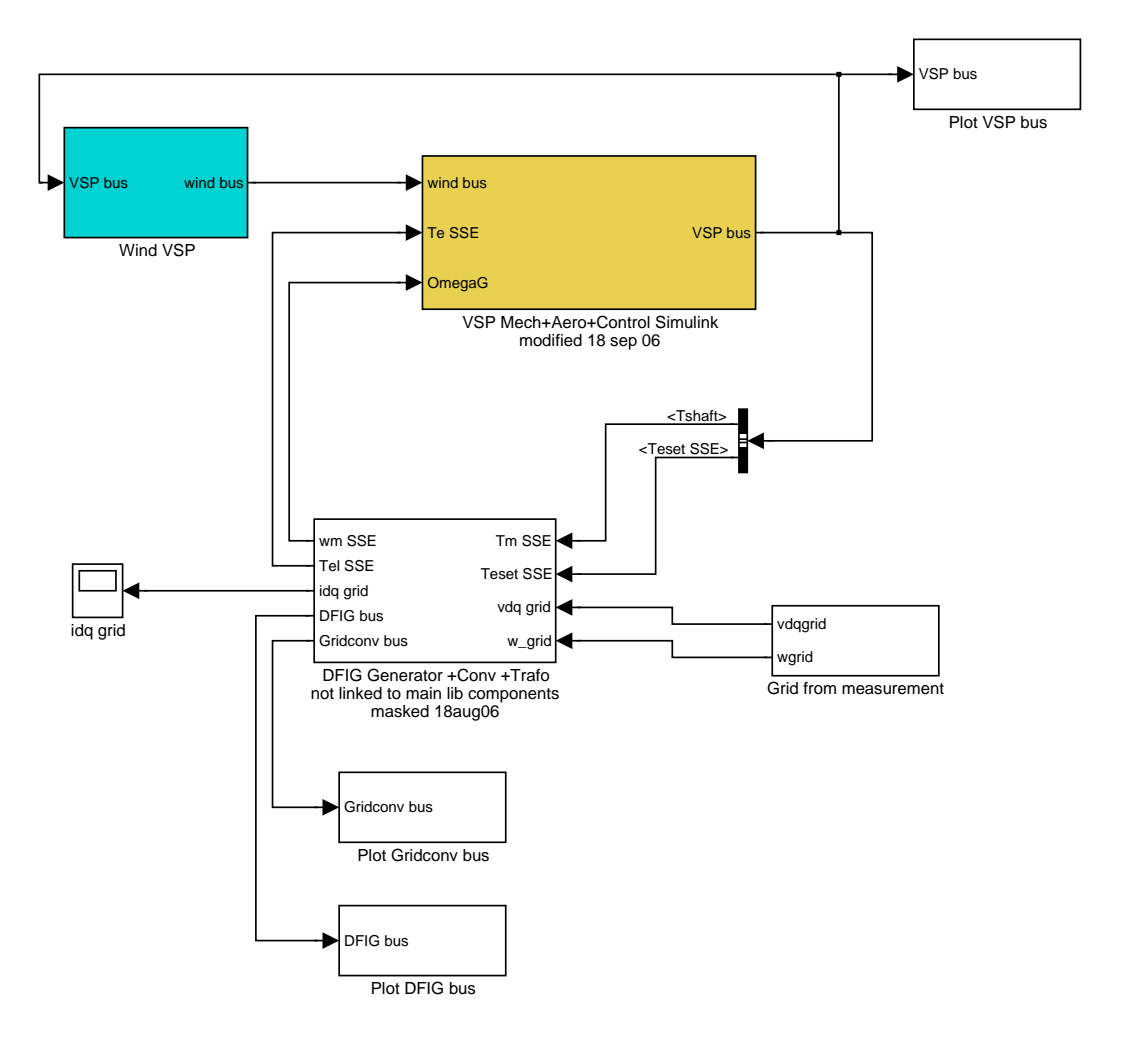


Figure 2: Simulink model main diagram

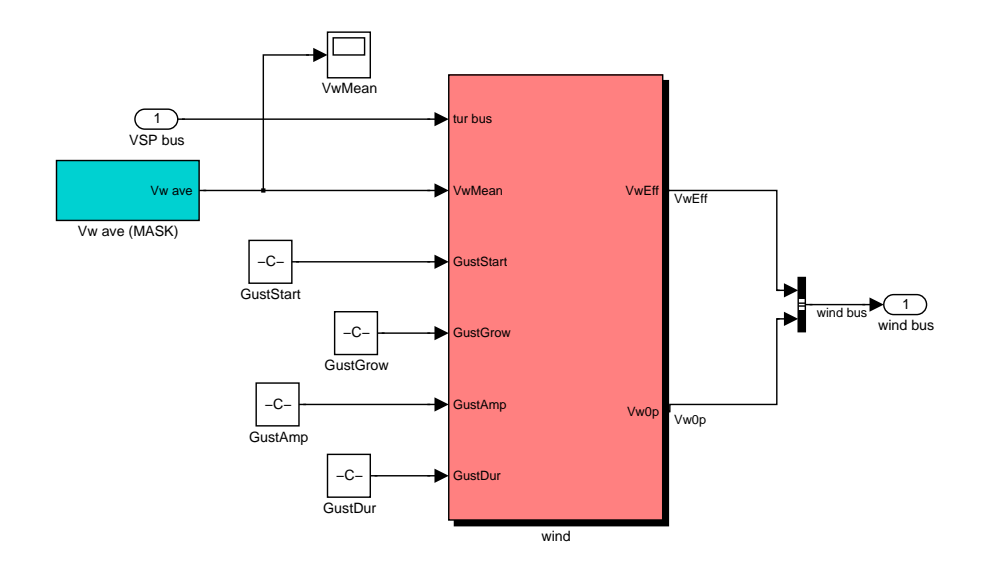


Figure 3: Simulink wind model diagram

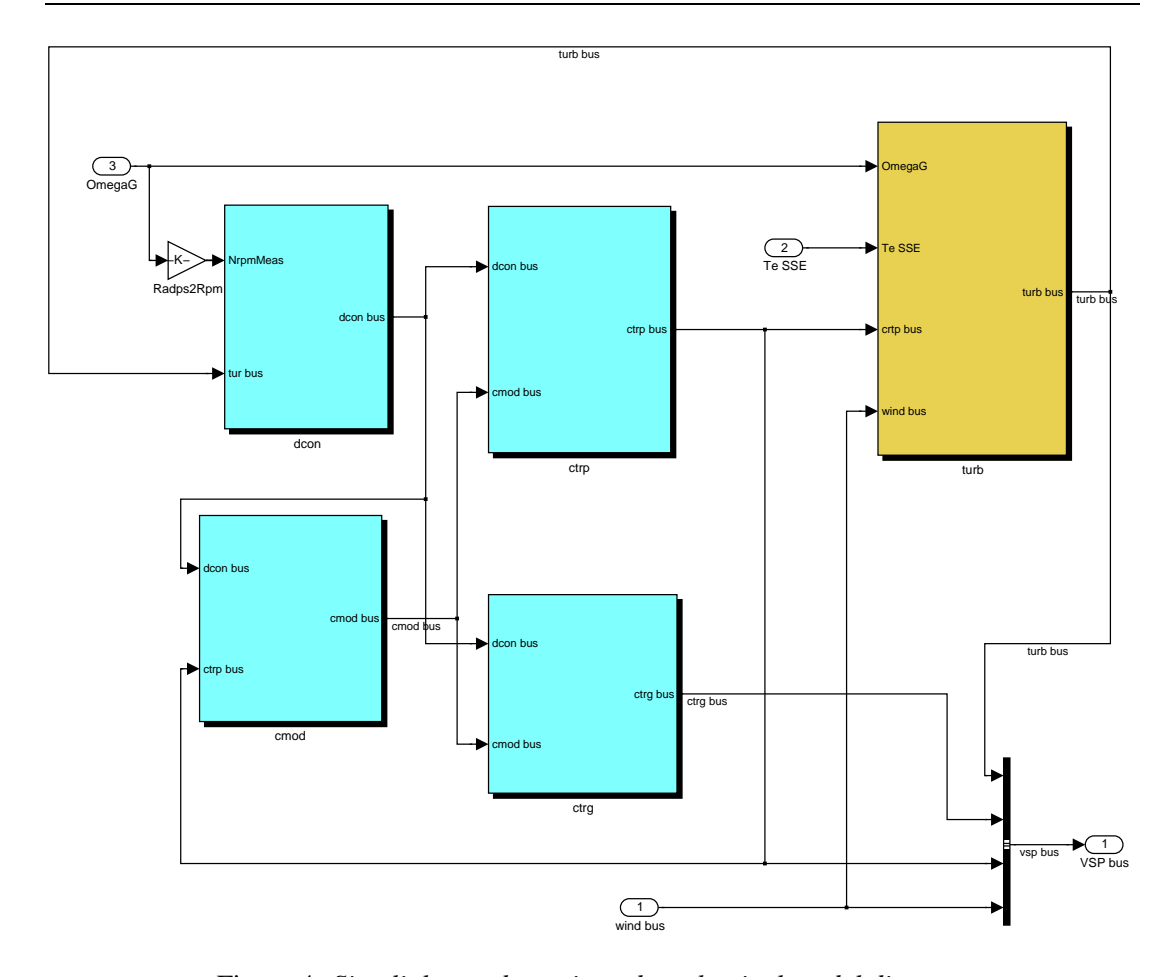


Figure 4: Simulink aerodynamic and mechanical model diagram

Figures 4 shows the aerodynamic, mechanical, pitch and speed control submodels. The original Erao-2 submodels have been re-programmed. The functionality of the old and new version is the same. The original Erao-2 version consisted of S-Functions (a special type of Matlab functions, structured to be included as part of a Simulink model). The problems with S-Functions are:

- user-unfriendlyness: the code is not accessable through the Simulink graphical interface;
- increased simulation time: Simulink code is faster than embedded Matlab code;
- · difficult debugging.

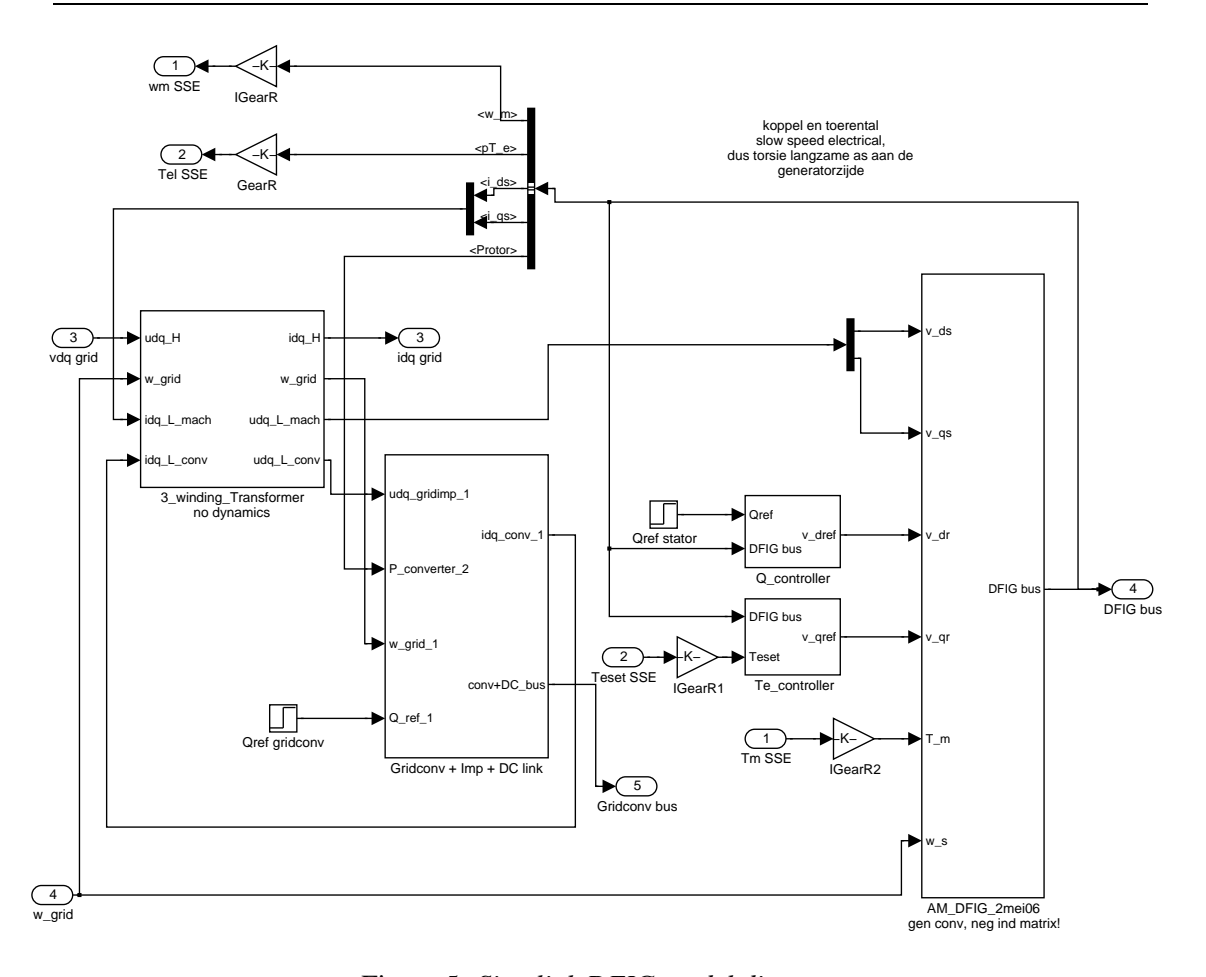


Figure 5: Simulink DFIG model diagram

Figure 5 gives the main submodels of the DFIG electrical system. Since the JWT turbine does not include a three winding transformer (generator and grid side converter operate at the same voltage), the dynamic model of the three winding transformer present in the NM92 electrical system was replaced by a contant voltage and current ratio.

The rotor converter controls the stator reactive power controller and the generator torque. Both consist of a master and a slave control loop. The slave determines the rotor current in the d (reactive power) or the q (torque) direction. This is represented by figure 6 and 7). To prevent initial transients, the controllers are switched on with a delay.

The grid converter controls the DC link voltage and the grid converter reactive power. A similar master-slave configuration on the d and q grid current is used.

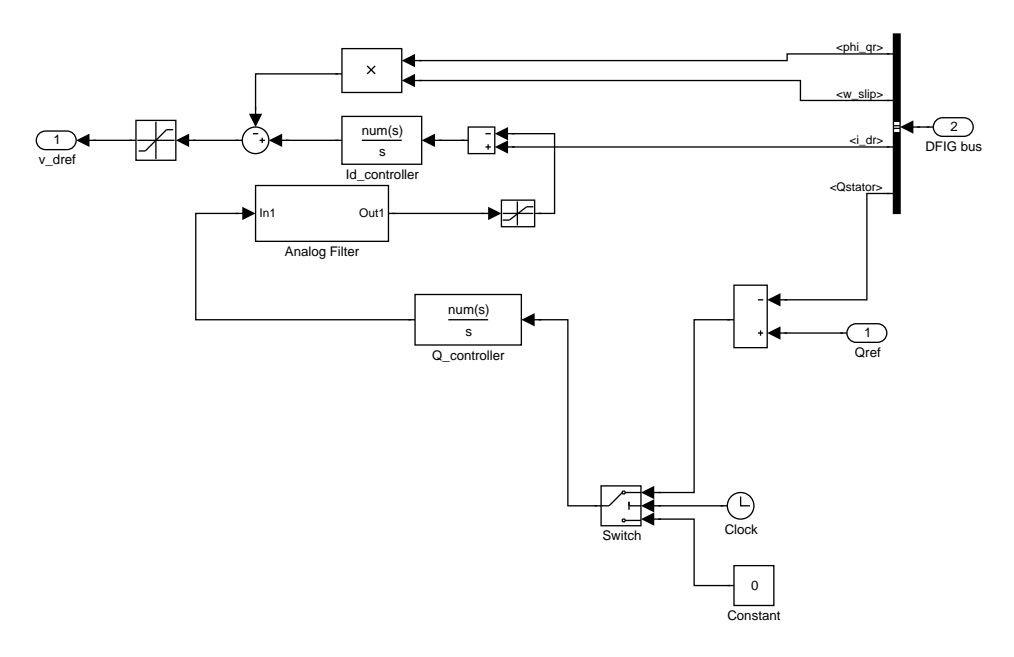


Figure 6: Simulink reactive power controller model diagram

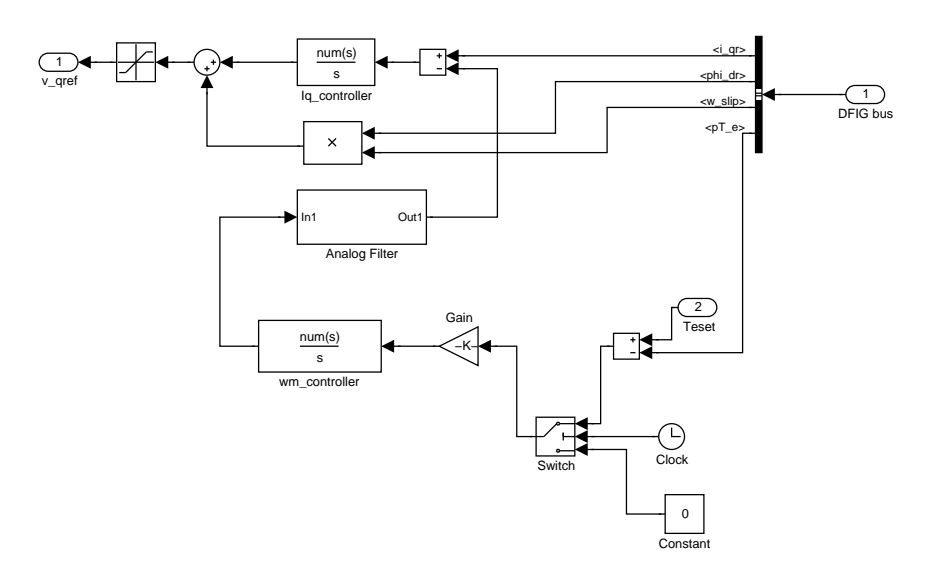


Figure 7: Simulink torque controller model diagram

# 5 JWT VSP-DFIG WIND TURBINE MODEL VALIDATION

The JWT measurements in the IEA Annex XXI data base comprise three sets of measurement:

- 1. normal operation, consisting of a low, half and full power measurement;
- 2. a symmetrical and an unsymmetrical voltage dip;
- 3. a disconnection.

The measurements have been performed by the Department of Electric Power Engineering of Chalmers University of Technology, Goteborg, Sweden. The measurement frequency is 2048 Hz. The normal operation measurements are 180 seconds long, the voltage dip measurements are 10 seconds long. The disconnection will not be part of the validation because it requires specific turbine data which was not available.

#### 5.1 Normal operation

Table 2 lists the variables measured during normal operation. The measurements do not include mechanical quantities. This limits the validation of the VSP turbine model to the electrical part.

Table 2: Measured signals of the JWT turbine

$u_1, u_2, u_3$	stator phase voltages
$i_1, i_2, i_3$	total currents currents
$ir_1, ir_2, ir_3$	converter currents grid side
$irr_1, irr_2, irr_3$	converter currents rotor side
ws	wind speed
pa	pitch angle
rpm	rotor speed

Figure 8 shows the location of the JWT turbine measurements (the stator current is is not measured but is calculated from the total current i and the grid converter ac current ir). Wind speed, pitch angle and rotor speed are not measured independently but are taken from the wind turbine data acquisition system. The accuracy of these signals is uncertain. The electrical measuremens are instantaneous values. There was no information on filtering of the signals.

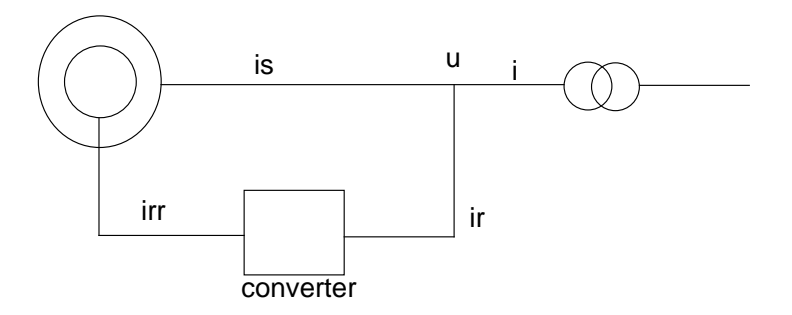


Figure 8: JWT turbine location of measurements

#### 5.2 Full power measurement

Prior to simulation of the full power case, the measurement is checked, the active and reactive power are calculated, the symmetry of the voltage and current measurements is checked and the d- and q-axis values of voltages and currents are calculated.

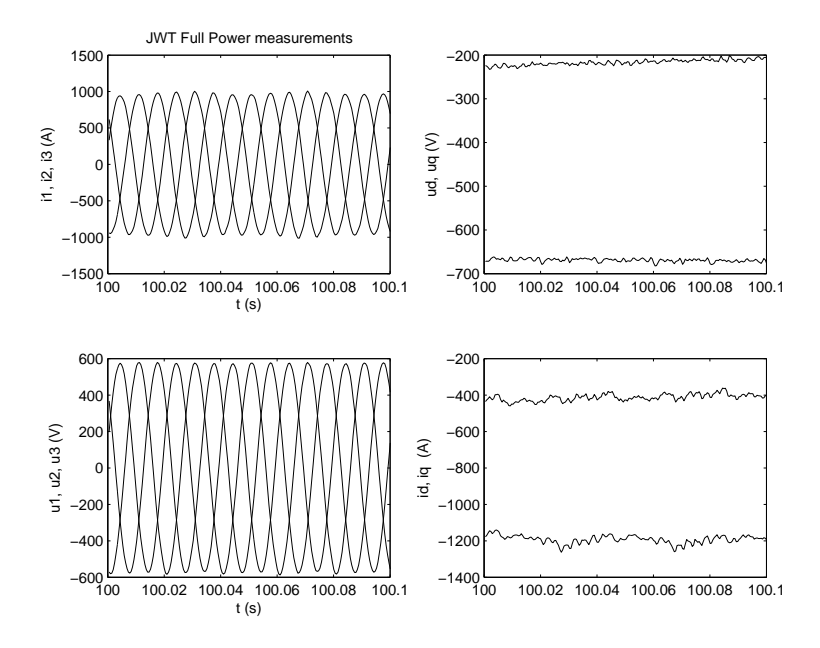


Figure 9: JWT turbine - Full Power - measurement: voltages and currents

Figure 9 shows a 100 ms section taken from the full power measurement. The instantaneous phase voltages and instantaneous total currents (sum of stator current and grid side converter current) are shown on the left hand side. From these values, assuming symmetrical conditions, the instantaneous dq-values are calculated (figure 9, right hand side). The unbalance or measurement inaccuracy in the measured voltage is between -15 and 5 V (about 1%), which is in the range of the measurement error. The unbalance or measurement inaccuracy in the measured current is between -9 and 18 A (also about 1%).

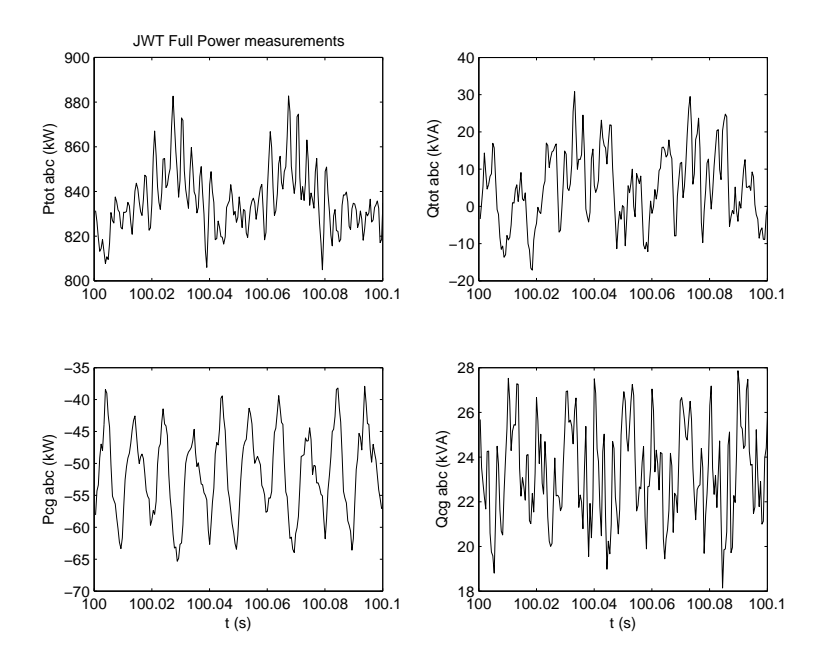


Figure 10: JWT turbine - Full Power - measurement: active and reactive powers

Figure 10 shows the total active and reactive power  $P_{tot}$  and  $Q_{tot}$  and the active and reactive power of the grid side converter  $P_{cg}$  and  $Q_{cg}$ , calculated from the measured grid phase voltages, the total currents and the grid side converter currents. The turbine produces maximum power (850 kW) and the converter power is practically zero (about 6% of the total power). This indicates a power margin at rated power, which in combination with a speed margin can cope with aerodynamic power variations and making life easier for the pitch control. This is a wind turbine design choice. The power variation at full power is about 80 kW, about 10% of the rated power. This corresponds to a variation of the voltage amplitude of about 3%. The average reactive power of the converter and the total reactive power are small, 20 kVA and about zero respectively. The rotor converter and the grid side converter control the stator reactive power and the grid converter reactive power to zero. This will also be chosen in the simulation.

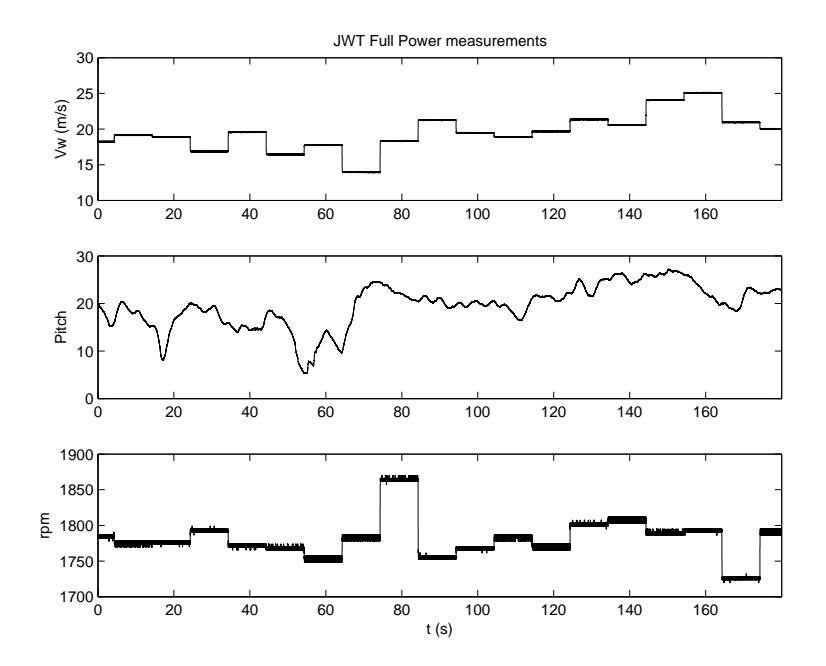


Figure 11: JWT turbine - Full Power - measurement: wind speed, pitch angle and rotational speed

Figure 11 shows the wind speed, pitch angle and rotational speed taken from the wind turbine data acquisition system. The wind speed and rotational speed display step changes, which indicates a poor measurement, if it is a measurement at all. Only the average value of the wind speed will be input for the simulation. The wind model calculates the rotor effective wind speed caused by random variation of the single point value, the variation of the wind speed over the rotor plane and the rotational sampling by the blades over the rotor plane. An accurate reproduction of time series of the measurement by the simulation will not be the aim of the simulation, as discussed previously: measurements and simulation results will be compared as auto power spectral density (APSD).

#### 5.3 Full power simulation

For the full power simulation the following choices have been made:

- the average single point wind speed is 19 m/s, the average value during the full power measurement;
- the aerodynamic and mechanical turbine model according to chapter 4;
- the electrical model according to chapter 4 with the following modification:
  - the turbine cable and the turbine transformer models are not included. This choice
    is made since the voltage is measured at the low voltage side of the turbine transformer and the JWT turbine does not include a three way transformer (the grid
    converter AC voltage equals the stator voltage);
- the input voltage is the moving average dq value of the measured instantaneous voltage (averaging time 10 ms) to exclude the high frequency harmonic noise;

- filters with a cut-off frequency of 10 Hz have been installed in the torque and reactive power master controller of the rotor side converter to prevent the feedback of the noise in the measured voltage;
- the rotor resistance has been increased by a factor 5 to compensate for additional losses not taken into account in the model (converter, transformer and cable losses; see also the remarks in Appendix A).

As discussed in the Constant Speed Wind Farm validation report [5], an assumption has to be made to calculate the d- and q-value of the voltage. If a constant frequency of 50 Hz is assumed, the voltage phasor rotates and the simulation is unstable. This can be the result of a significant mismatch between the actual and calculated voltage phasor angle, since the measurement is quite long and the error is integrated. A second cause for instability can be the controller design method which may not be suitable for a rotating voltage phasor. If instead of constant frequency the q-component of the voltage is assumed to be zero, i.e. constant voltage phasor angle with variable phasor rotational speed, the simulation is perfectly stable. In the normal operation case simulations a constant voltage phasor angle will be used.

The next figures show the simulation results for the JWT turbine during full power operation. The noise on the electrical signals is caused by the noise on the input voltage  $v_{ds}$ , figure 14. The low frequency oscillations in the wind speed  $V_w E_{ff}$  and the aerodynamic torque  $T_a$  are caused by tower passage and rotational sampling of the blades.

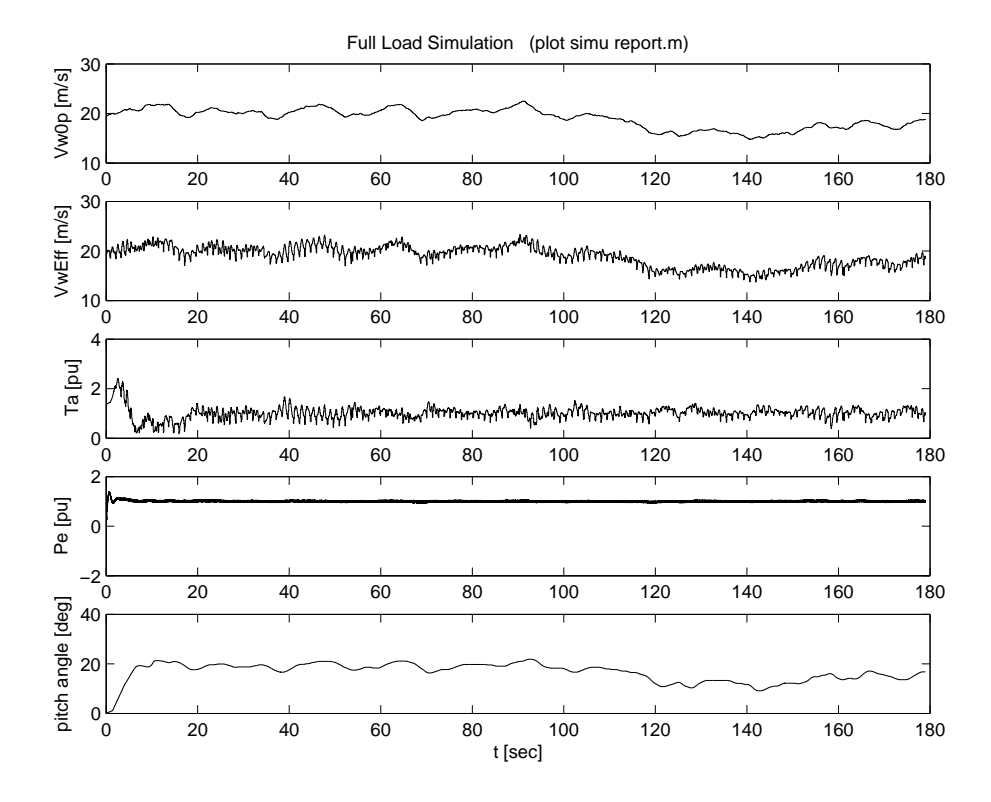


Figure 12: Full power - simulation: Rotor plane wind speed, rotor effective wind speed, aerodynamic torque, total electric power and pitch angle

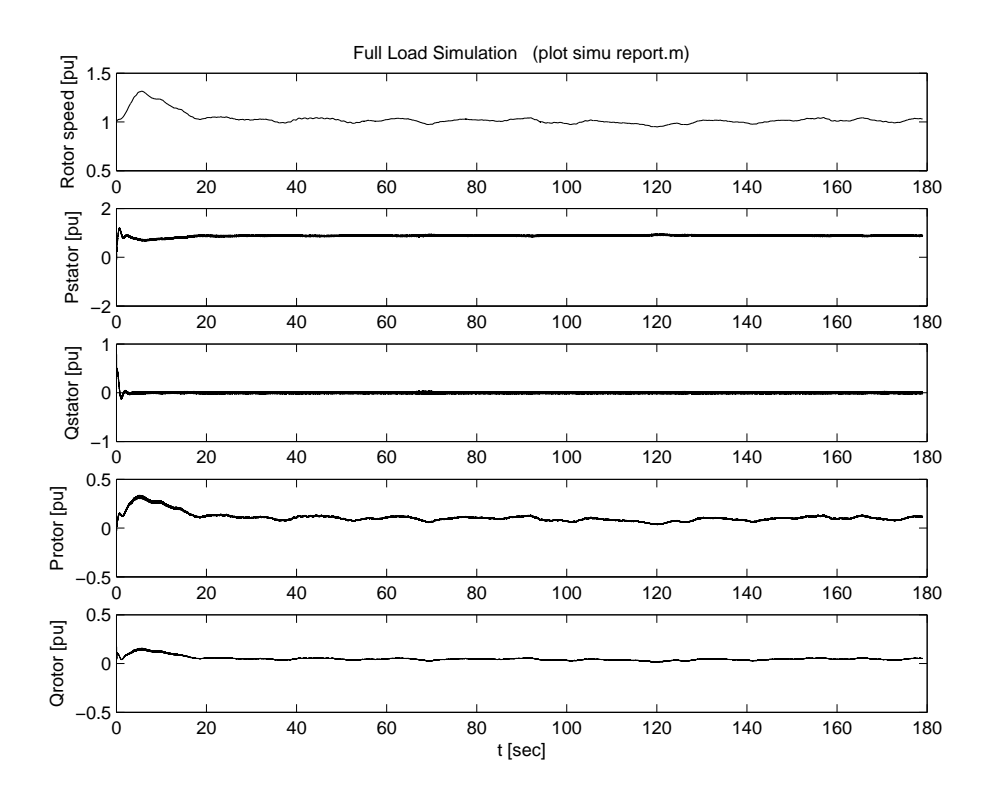


Figure 13: Full power - simulation: rotor speed, stator power, stator reactive power, rotor power and rotor reactive power

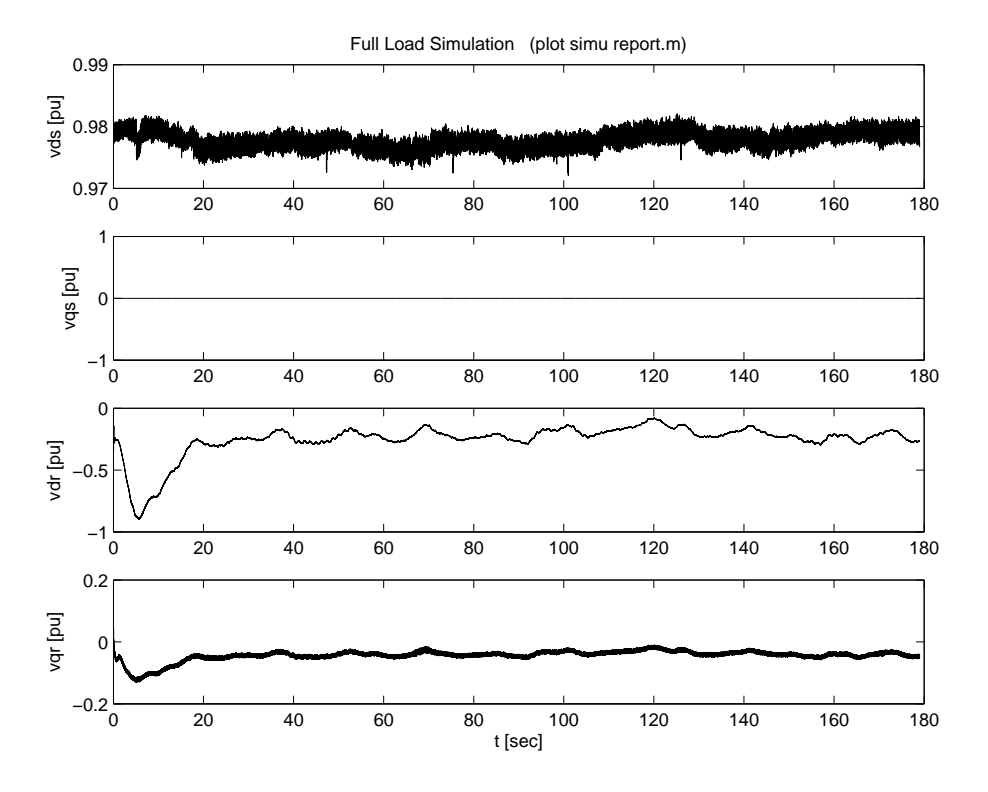


Figure 14: Full power - simulation: stator d- and q-voltage, rotor d- and q-voltage

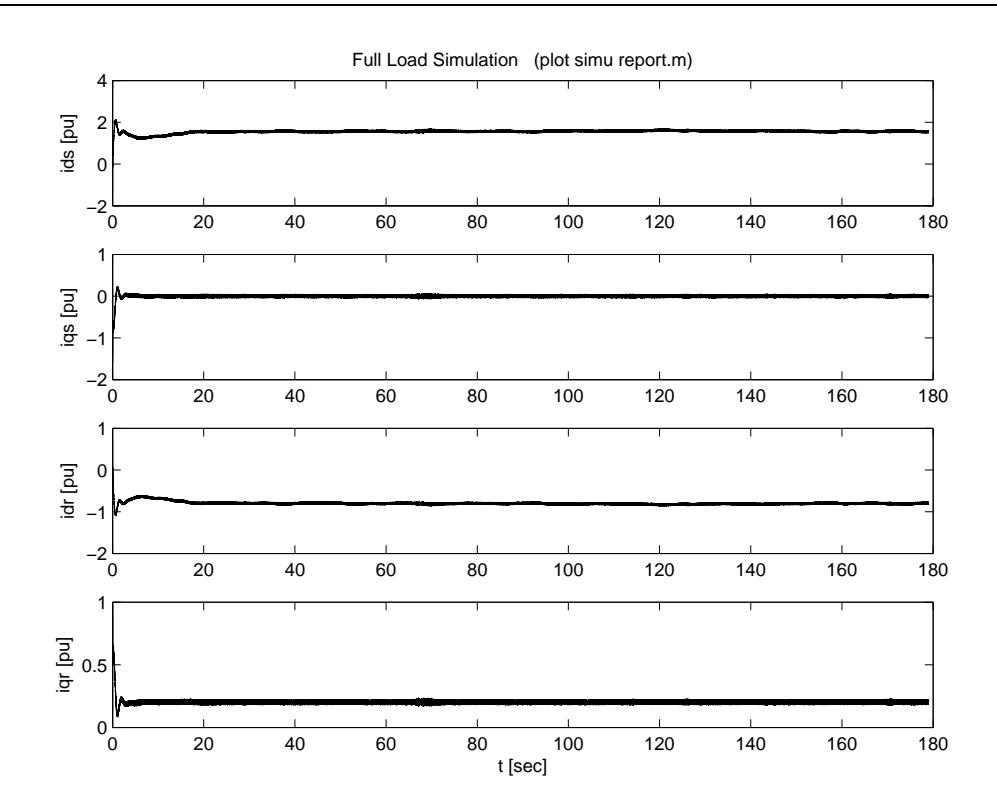


Figure 15: Full power - simulation: stator d- and q-current, rotor d- and q-current

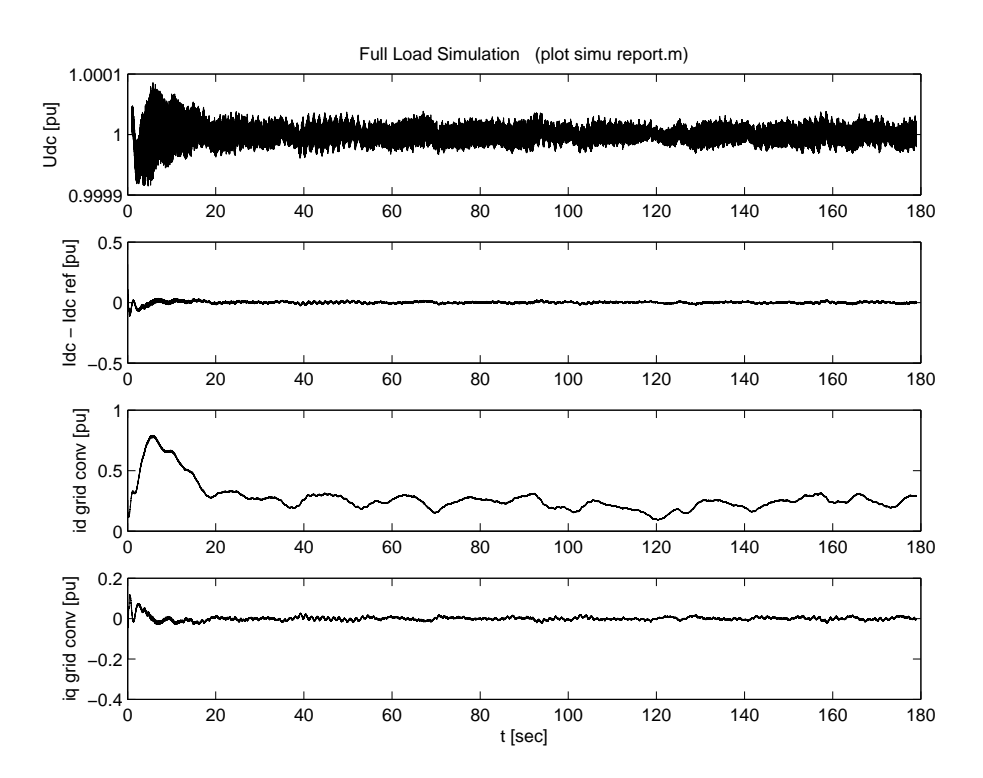


Figure 16: Full power - simulation: DC voltage deviation from setpoint, DC current deviation from setpoint, grid side converter d- and q-current

#### 5.4 Comparing full power measurement and simulation results

Since comparing measurement and simulation in the time domain will not give much information on the performance of the model, due to the difference in rotor effective wind speed in measurement and simulation, measurement and simulation are compared in the frequency domain. The APSD of the active and reactive powers at the measurement locations are compared. This method is also applied in the Chalmers study [10]. Since the rated power of the simulated turbine is different from the JWT turbine, the spectra of the simulations are scaled with the square of the rated power ratio to make the APSDs comparable.

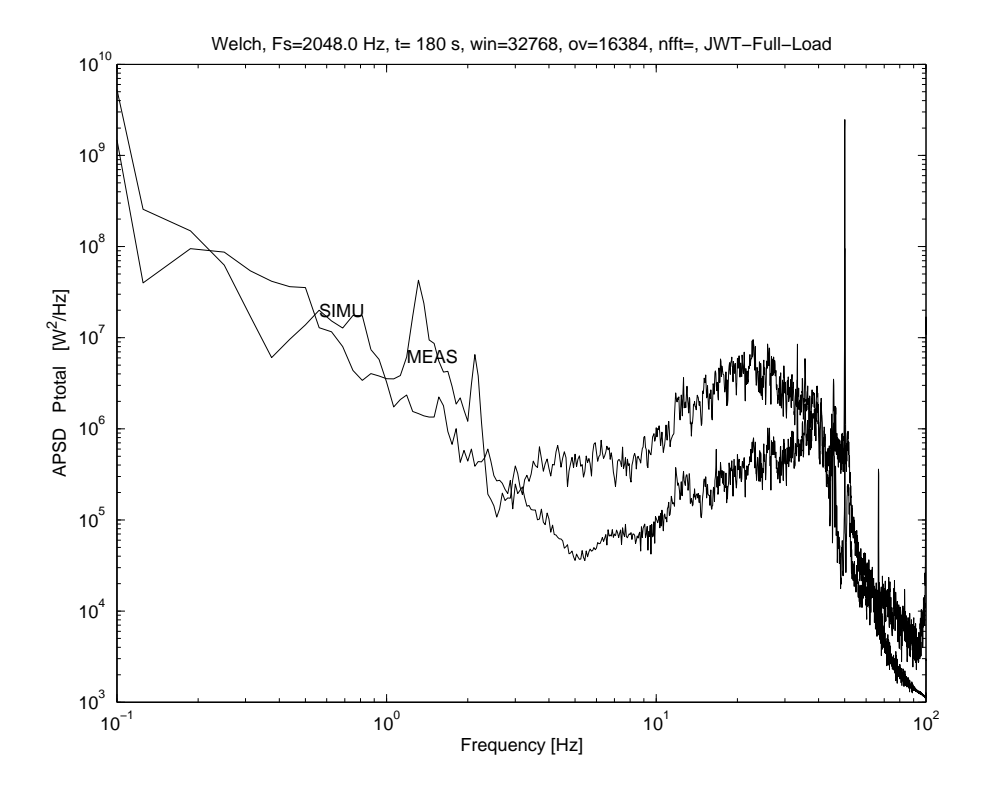


Figure 17: Full power - APSD: Total Power - measurement (MEAS) and simulation (SIMU)

Figure 17 compares the APSDs of the total power for normal operation at full power:

- in the frequency range 0.1-3 Hz, the variabilty in simulation and measurement is similar;
- the peaks at 1.3 and 2.2 Hz in the measurement are missing in the simulation.
- in the frequency range 3-40 Hz the variabilty in simulation is less than in the measurement;
- from 40-100 Hz simulation and measurements are more or less similar again.

The rotational speed of the JWT is 31 rpm (full power) or 0.52 Hz. So the peaks at 1.3 and 2.2 Hz in the measurement are not linked to  $n \cdot 3P$  (1.56, 3.12 Hz etc.). Possible causes could be mechanical eigenfrequencies of the drive train or the blades. Since the turbine parameters in the simulation represent a turbine of the VSP-DFIG type but not the JWT turbine, it is not surprising that the peaks in the measurement are not reproduced in the simulation.

The next figures compares the APSDs of stator power, grid side converter power, total reactive power, stator reactive power and grid side converter reactive power. Surprisingly differences

between measurement and simulation are larger for the stator power and grid converter power than for the total power, indicating cancellation of oscillations in the measurement. The differences are not that big however, about a factor 10, so in the actual signals  $\sqrt{10}$ .

The APSDs of the total reactive power (figure 20) show a different result than the APSDs of the total power:

- in the frequency range 0.1-1 Hz, the variability in simulation is much higher than in the measurement;
- in the frequency range 1-6 Hz, the variabilty in simulation and measurement is similar;
- in the frequency range 6-30 Hz the variabilty in simulation is higher than in the measurement.

The reactive power control for a DFIG consists of two independent controllers, one for the stator and one for the grid side converter reactive power. The first controller operates on the rotor current, the second on the grid converter current. The reactive power control in the simulation clearly differs from the control in the JWT turbine. The stator reactive power controller in the simulation was designed by TUD using the IMC method [7]. The grid converter reactive power controller is based on a master-slave design controlling the current phasor component perpendicular to the voltage phasor. The dynamics of both controllers depend on the dynamic properties of the system as well as the controller design. The controllers in the model clearly differ from the controllers in the JWT turbine. Figures 21 and 22 show that both reactive power controllers contribute to the difference.

The peaks at 1.3 and 2.2 Hz are present in all measurements. The simulation of the grid side converter reactive power shows peaks at 0.8, 1.6, 2.4, 3.2 and 4.0 Hz which are not present in the measurement. The rotor speed in the simulation is 1.7 rad/s, so 0.8 Hz is the number of blades times the rotational frequency. It is a bit unexpected that this frequency only occurs in the grid side converter reactive power but not in the APSDs of the powers. The grid side converter reactive power controller in the model feeds variations in the rotational speed back to the reactive power.

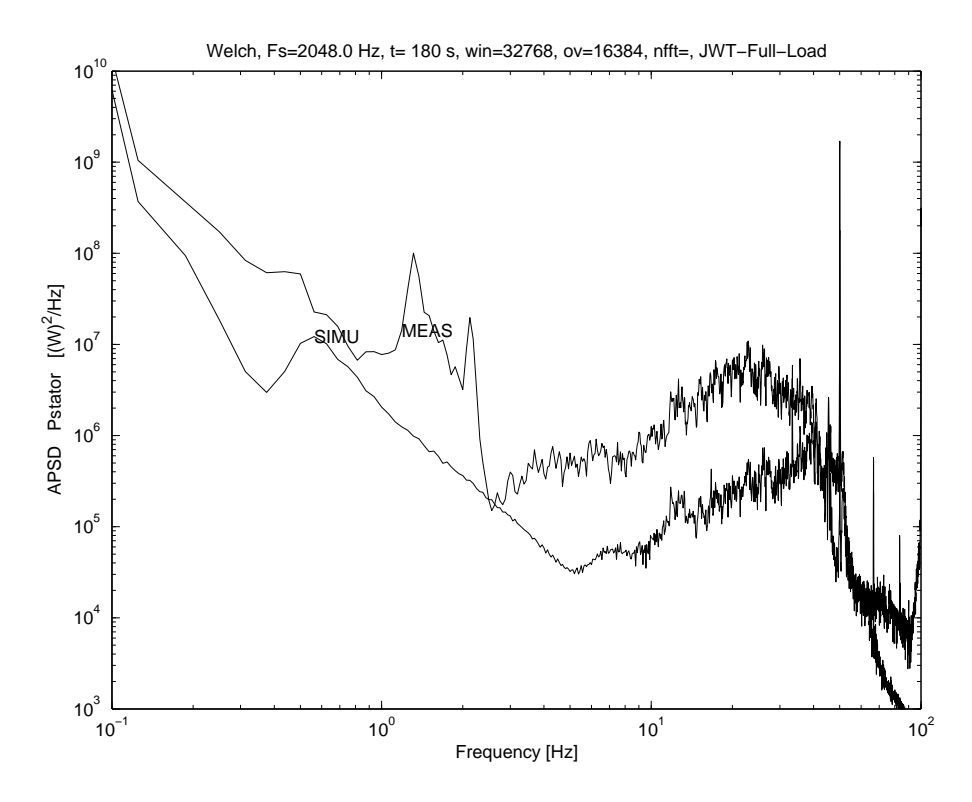


Figure 18: Full power - APSD: Stator Power - measurement (MEAS) and simulation (SIMU)

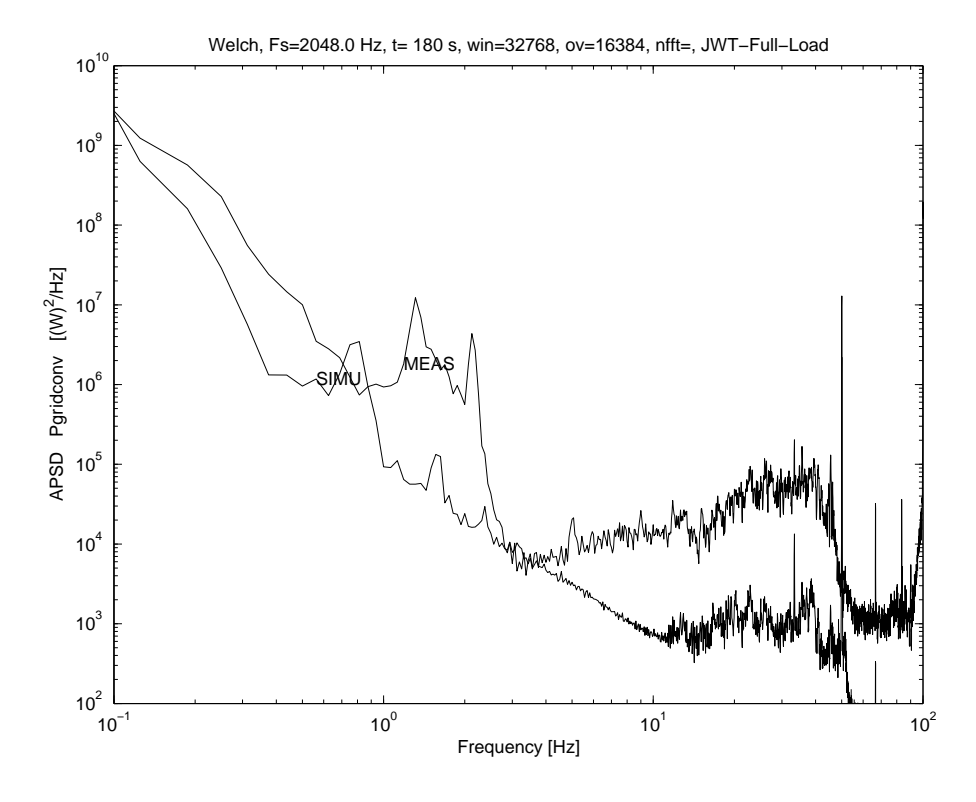


Figure 19: Full power - APSD: Grid side converter Power - measurement (MEAS) and simulation (SIMU)

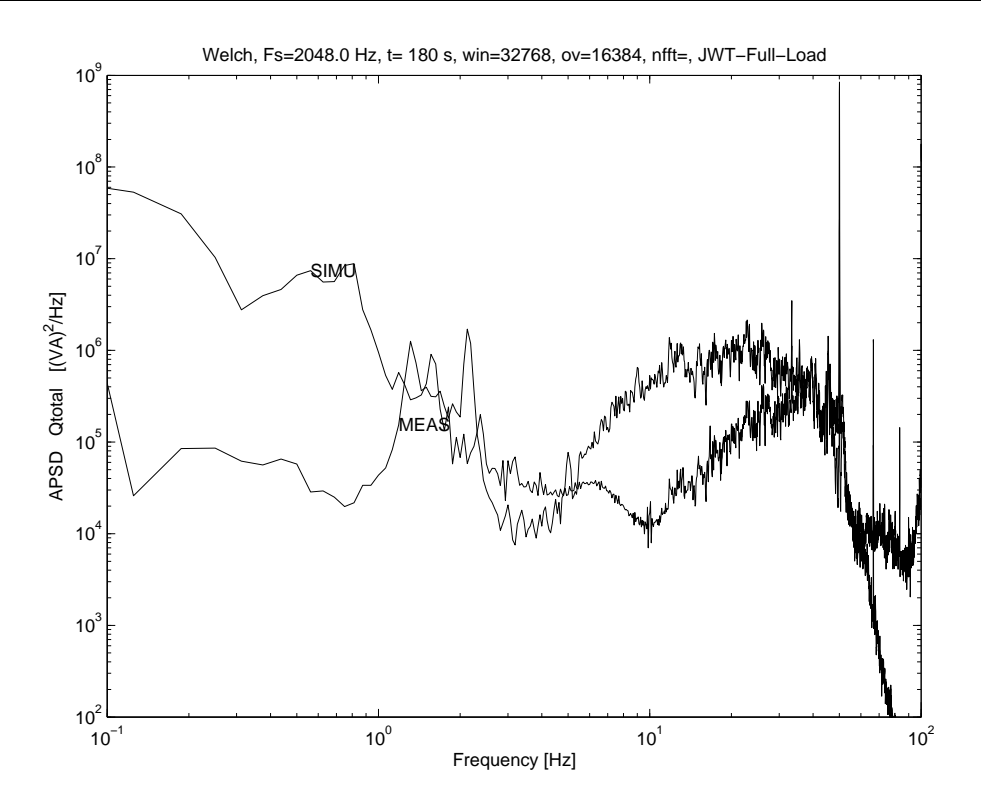


Figure 20: Full power - APSD: Total Reactive Power - measurement (MEAS) and simulation (SIMU)

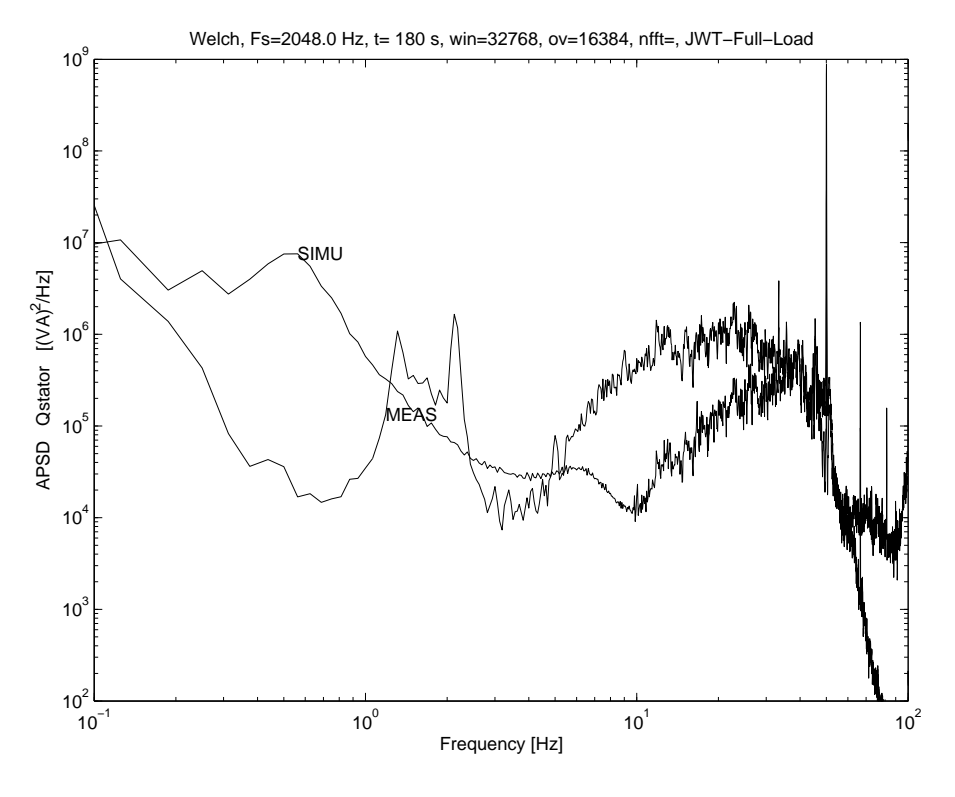


Figure 21: Full power - APSD: Stator Reactive Power - measurement (MEAS) and simulation (SIMU)

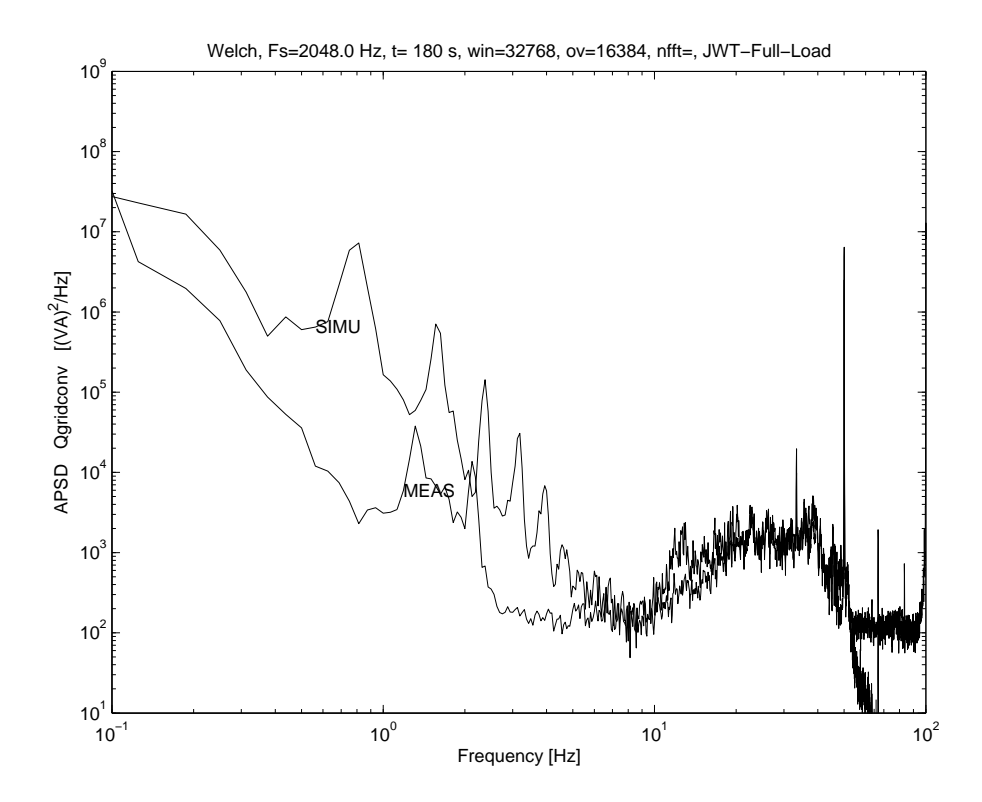


Figure 22: Full power - APSD: Grid side converter Reactive Power - measurement (MEAS) and simulation (SIMU)

# 5.5 Half power measurement

The half power measurement has been checked, the symmetry of the voltage and current measurements has been checked, the active and reactive power are calculated and the d- and q-axis values of voltages and currents are calculated.

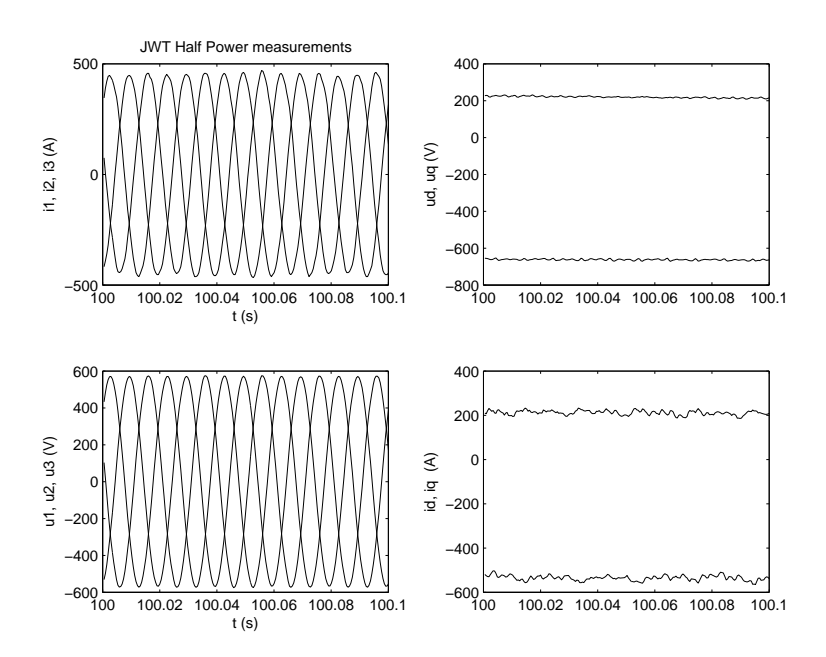


Figure 23: JWT turbine - Half Power - measurement: voltages and currents

Figure 23 shows a 100 ms section taken from the half power measurement. The instantaneous phase voltages and total currents (sum of stator current and grid side converter current) are shown on the left hand side. From these values the instantaneous dq-vales are calculated (right hand side), assuming symmetrical conditions. The unbalance or measurement inaccuracy in the measured voltage is between -2 and 7 V (about 1%), which is in the range of the measurement error. The unbalance or measurement inaccuracy in the measured current is between -5 and 15 A (about 2.5%).

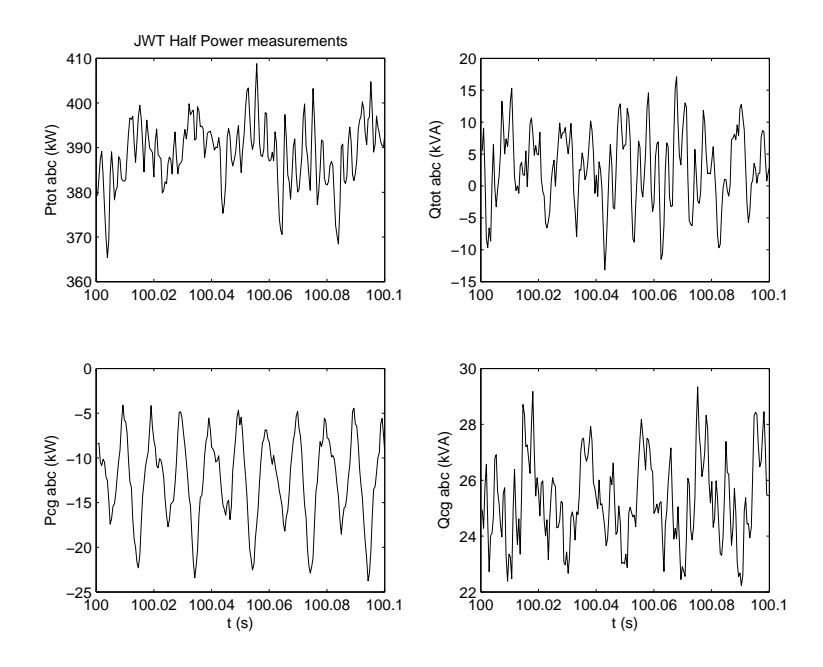


Figure 24: JWT turbine - Half Power - measurement: active and reactive powers

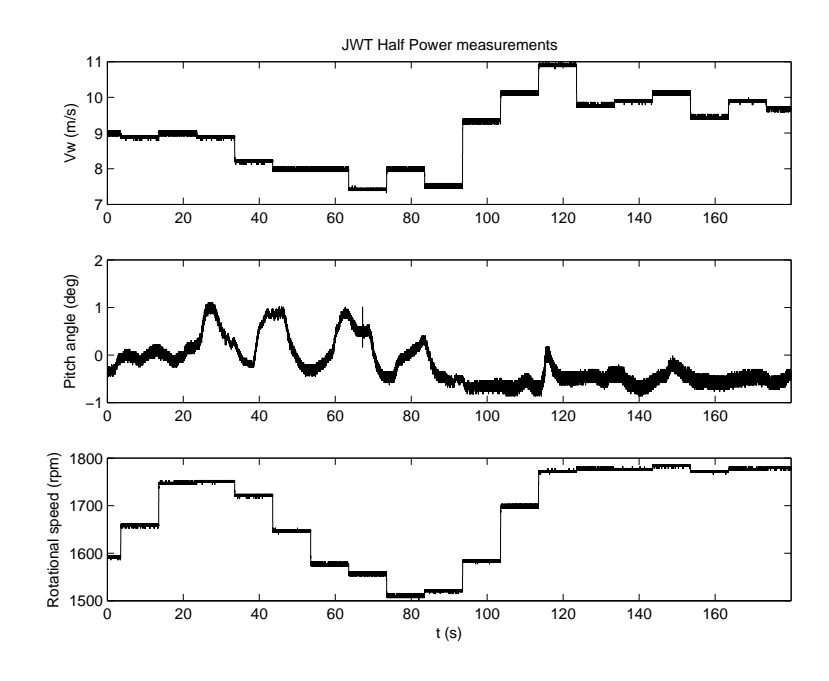


Figure 25: JWT turbine - Half Power - measurement: wind speed, pitch angle and rotational speed

Figure 24 shows the total active and reactive power  $P_{tot}$  and  $Q_{tot}$  and the active and reactive power of the grid side converter  $P_{cg}$  and  $Q_{cg}$ , calculated from the measured instantaneous grid phase voltages, the total currents and the grid side converter currents. The turbine produces about 390 kW and the converter power is -12 kW. The average reactive power of the converter and the total reactive power are small, 25 kVA and about zero respectively. The rotor converter and the grid side converter are controlled in such a way that the stator reactive power and the grid converter reactive power are practically zero. This will also be chosen in the simulation.

Figure 25 shows the wind speed, pitch angle and rotational speed taken from the wind turbine data acquisition system. The speed is in the range of 1700 rpm. The wind speed and rotational speed display step changes, which indicates a poor measurement. Only the average value of the wind speed will be input for the simulation.

#### 5.6 Half power simulation

For the half power simulation the following choices have been made;

- the average single point wind speed is 9 m/s, the average value during the half power measurement;
- the input voltage is the moving average dq-value of the measured instantaneous voltage (averaging time 10 ms) to exclude the high frequency harmonic noise. Constant voltage phasor angle is assumed;
- the choices concerning the model are equal to those for the full power simulation, see section 5.3.

The following five figures show the simulation results for the JWT turbine during half power normal operation. The high frequency noise on the electrical signals is caused by the noise on the input voltage  $v_{ds}$ , figure 28. The low frequency oscillations in the wind speed  $V_w E_{ff}$  and the areodynamic torque  $T_a$  are caused by tower passage and rotational sampling of the blades.

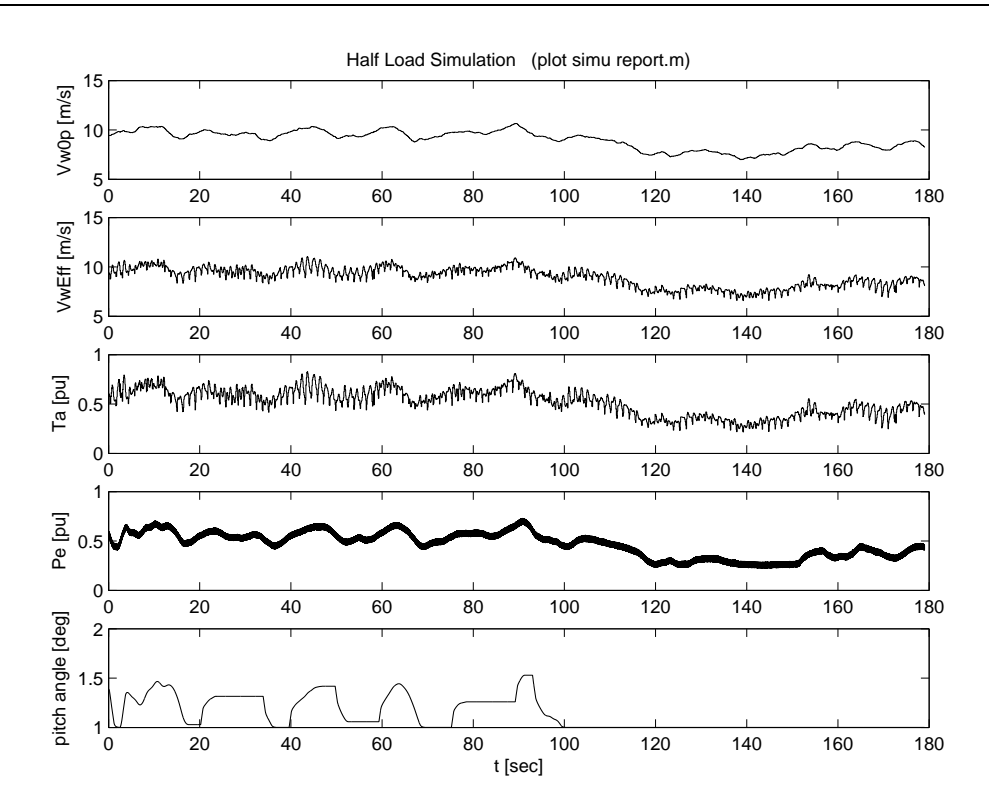


Figure 26: Half power - simulation: Rotor plane wind speed, rotor effective wind speed, aero-dynamic torque, total electric power and pitch angle

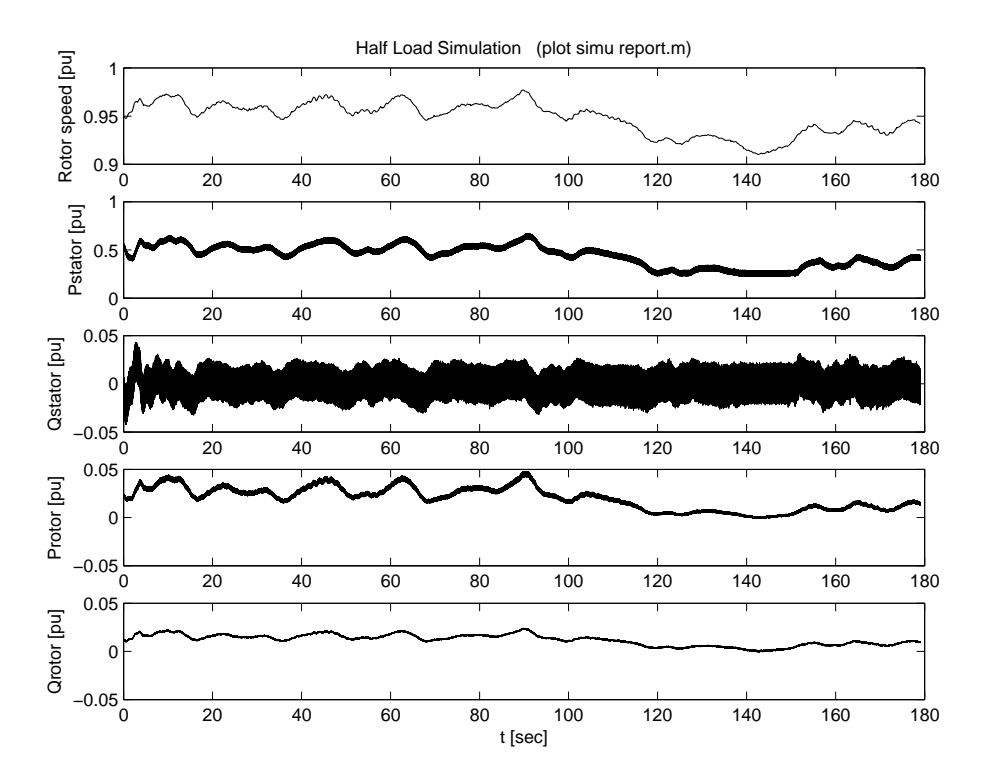


Figure 27: Half power - simulation: rotor speed, stator power, stator reactive power, rotor power and rotor reactive power

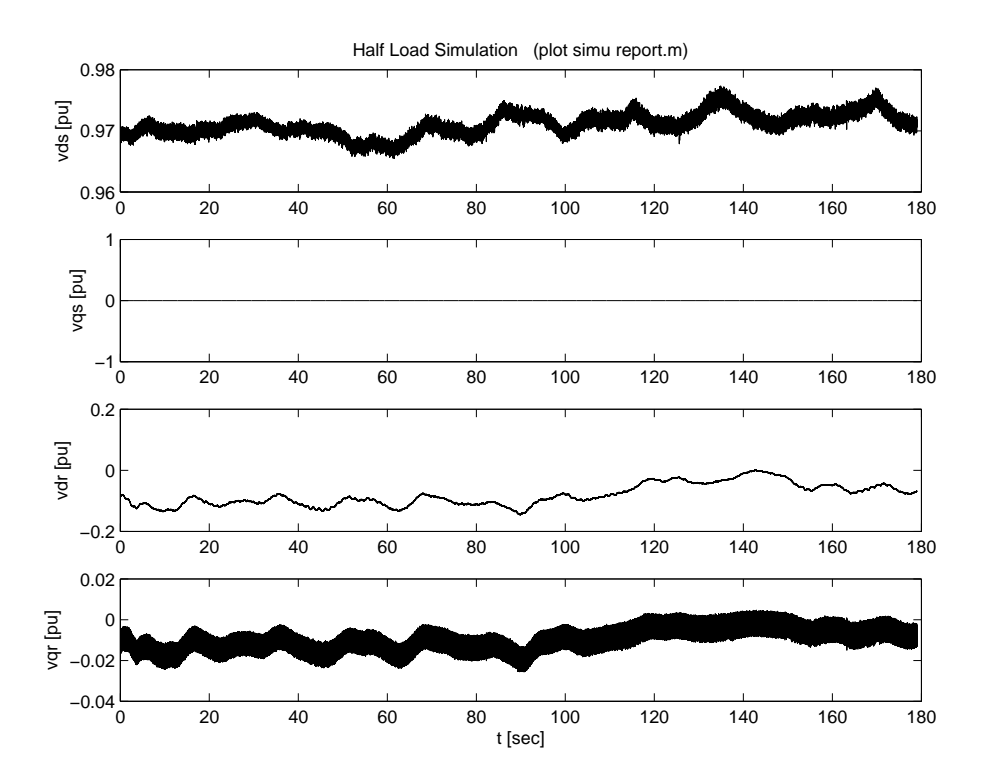


Figure 28: Half power - simulation: stator d- and q-voltage, rotor d- and q-voltage

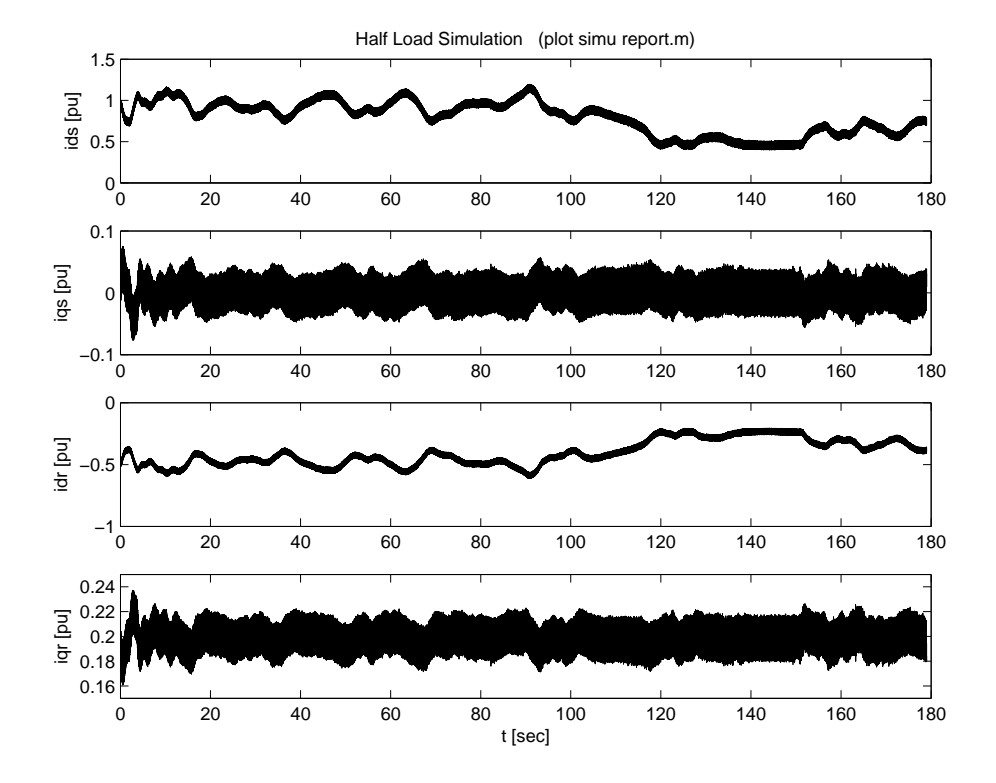


Figure 29: Half power - simulation: stator d- and q-current, rotor d- and q-current

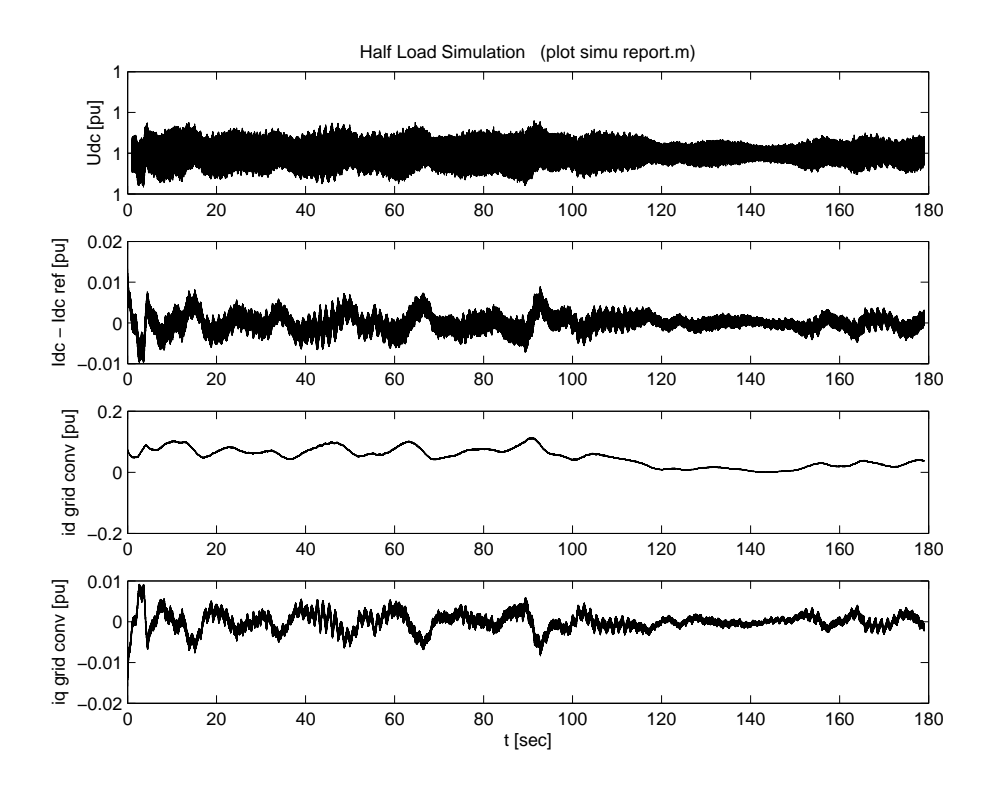


Figure 30: Half power - simulation: DC voltage deviation from setpoint, DC current deviation from setpoint, grid side converter d- and q-current

#### 5.7 Comparing half power measurement and simulation results

Figure 31 compares the APSDs of the total power for normal operation at half power:

- in the frequency range below 2 Hz, the variabilty in the simulation is similar to the measurement;
- in the frequency range 2-10 Hz, the variability in the simulation is less than in the measurement:
- the peak at 1.4 Hz in the measurement is missing in the simulation, the simulation produces a peak at about 0.4 Hz;

Figures 32 and 33 compare the APSDs of stator power and grid side converter power respectively. The differences between measurement and simulation are basically the same as for the total power APSDs.

Figures 34 to 36 compare the APSDs of total reactive power, stator reactive power and grid side converter reactive power. The differences in the low frequency range are much larger than for the active powers. The differences are attributed to a different reactive power controller design, as discussed in section 5.4.

The simulation of the grid side converter reactive power shows peaks at 0.75, 1.5, 2.2, 3.0 and 3.75 Hz which are not present in the measurement. These are multiples of the number of blades times the rotational frequency  $(n \cdot 3P)$ , similar to the full load case. Since the turbine parameters were not available can not be expected to reproduce the peaks in the measurements.

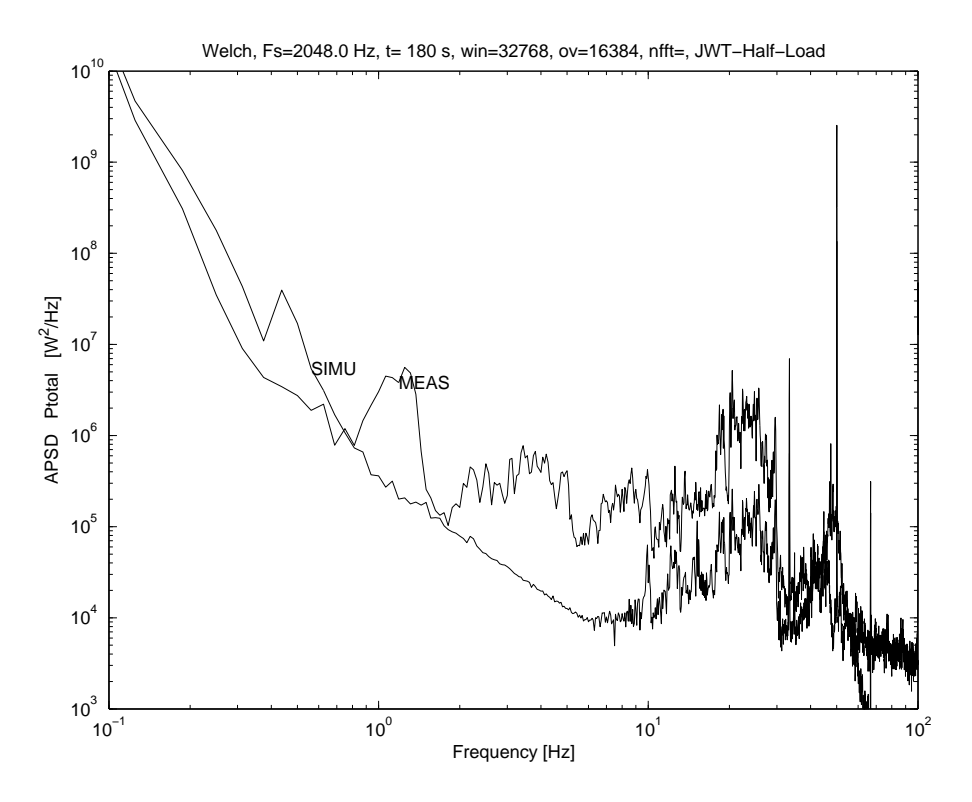


Figure 31: Half power - APSD: Total Power - measurement (MEAS) and simulation (SIMU)

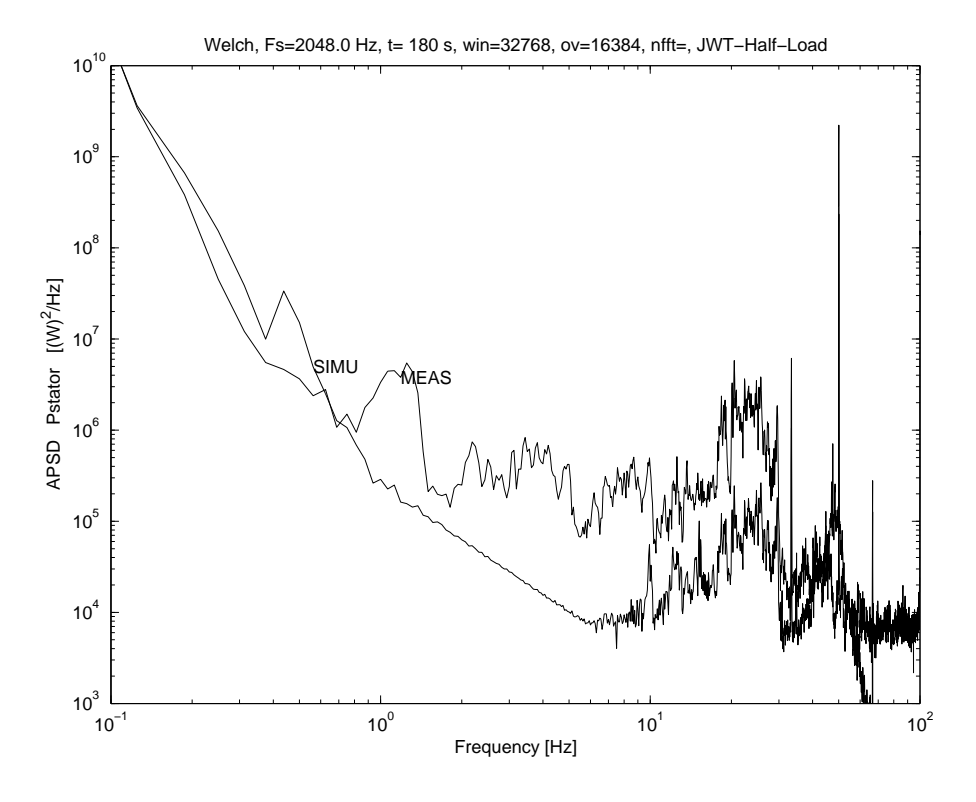


Figure 32: Half power - APSD: Stator Power - measurement (MEAS) and simulation (SIMU)

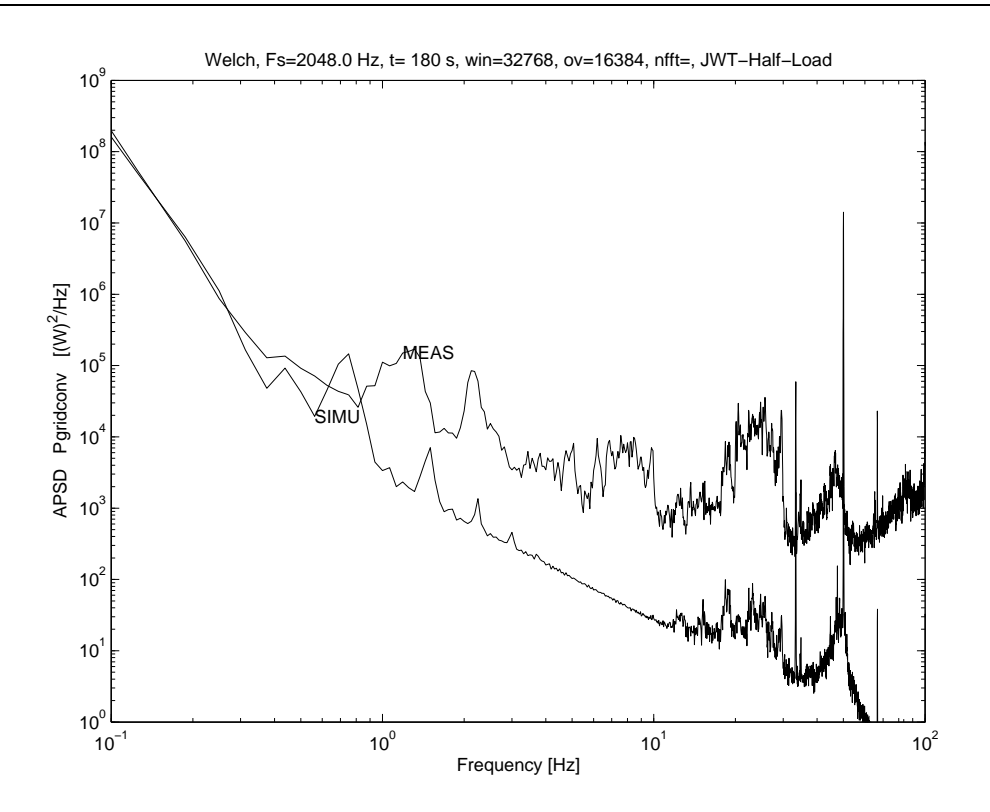


Figure 33: Half power - APSD: Grid side converter Power - measurement (MEAS) and simulation (SIMU)

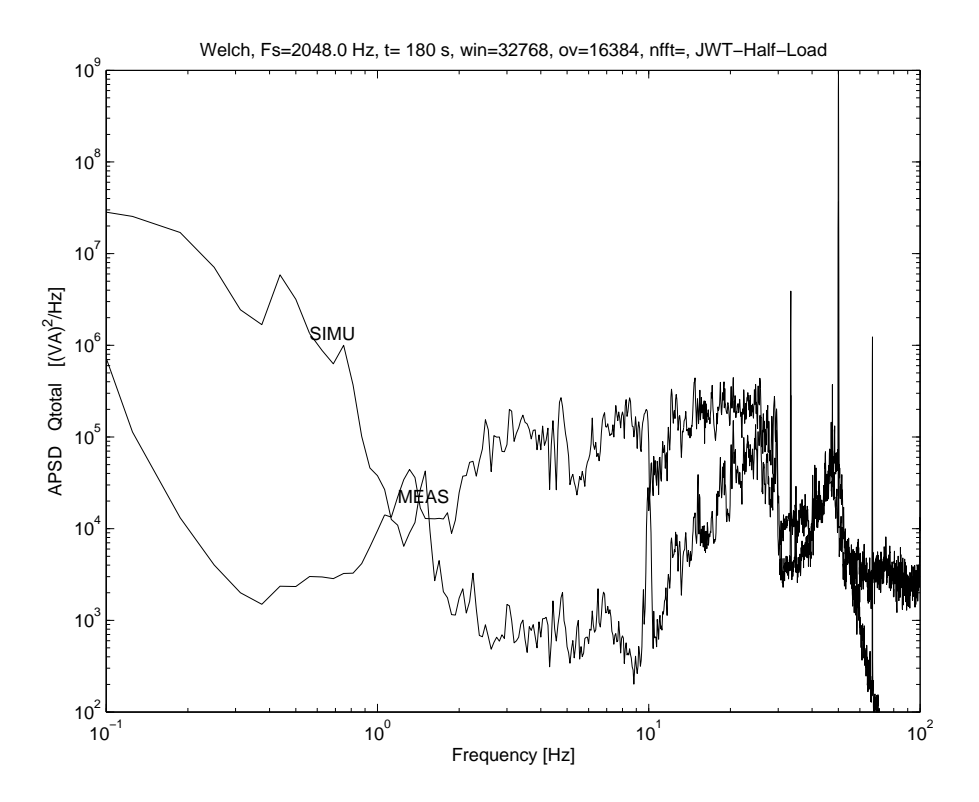


Figure 34: Half power - APSD: Total Reactive Power - measurement (MEAS) and simulation (SIMU)

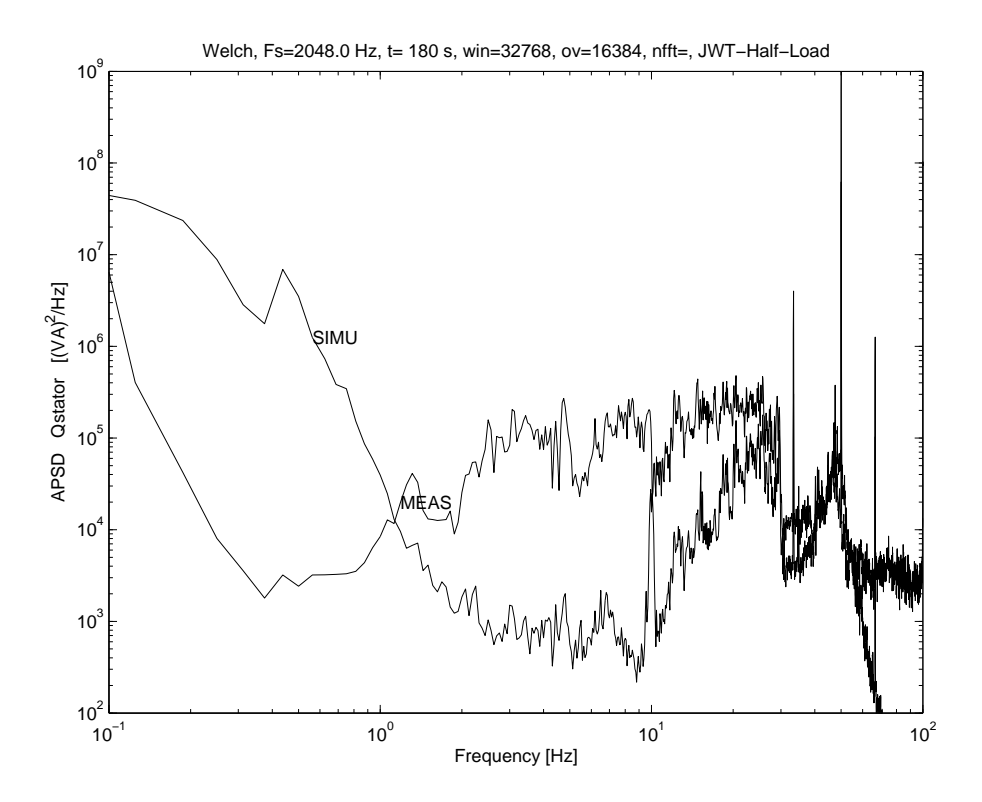


Figure 35: Half power - APSD: Stator Reactive Power - measurement (MEAS) and simulation (SIMU)

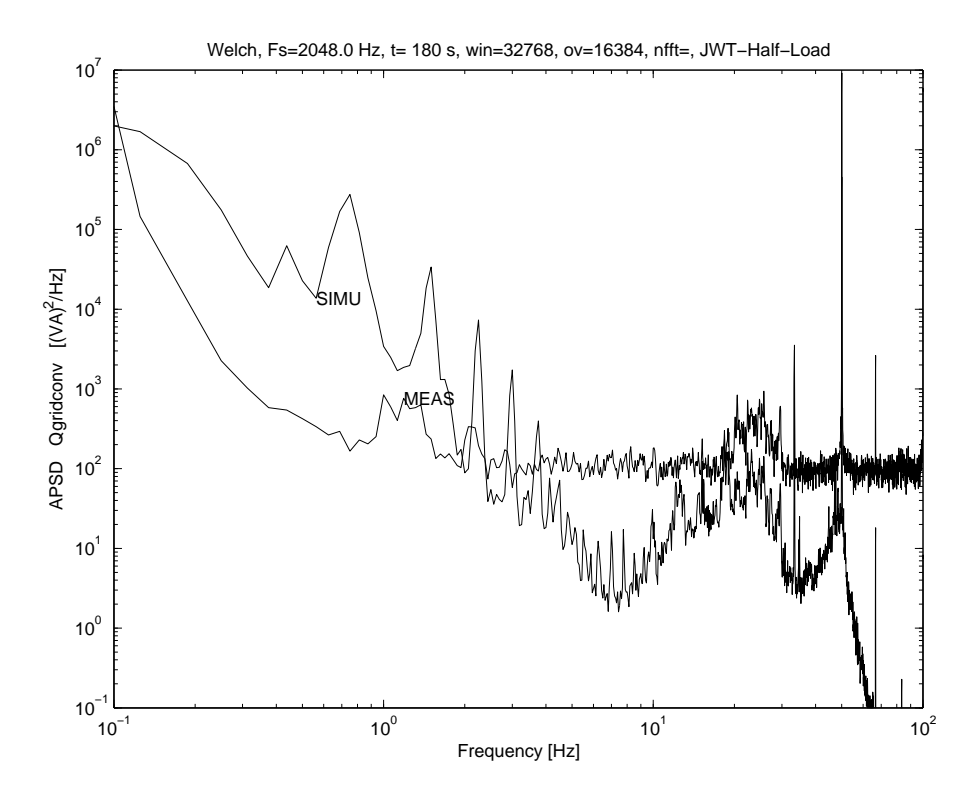


Figure 36: Half power - APSD: Grid side converter Reactive Power - measurement (MEAS) and simulation (SIMU)

### 5.8 Low power measurement

Figure 37 shows a 100 ms section taken from the half power measurement. The instantaneous phase voltages and total currents (sum of stator current and grid side converter current) are shown on the left hand side. From these values the instantaneous dq-vales are calculated (right hand side), assuming symmetrical conditions. The unbalance or measurement inaccuracy in the measured voltage is between -1 and 6 V (about 1%), which is in the range of the measurement error. The unbalance or measurement inaccuracy in the measured current is between -5 and 14 A, similar to the full and half load case, about 14%. This is a relatively high value. Since the absolute value is independent of the power the turbine produces, it is likely that it is a measurement inaccuracy.

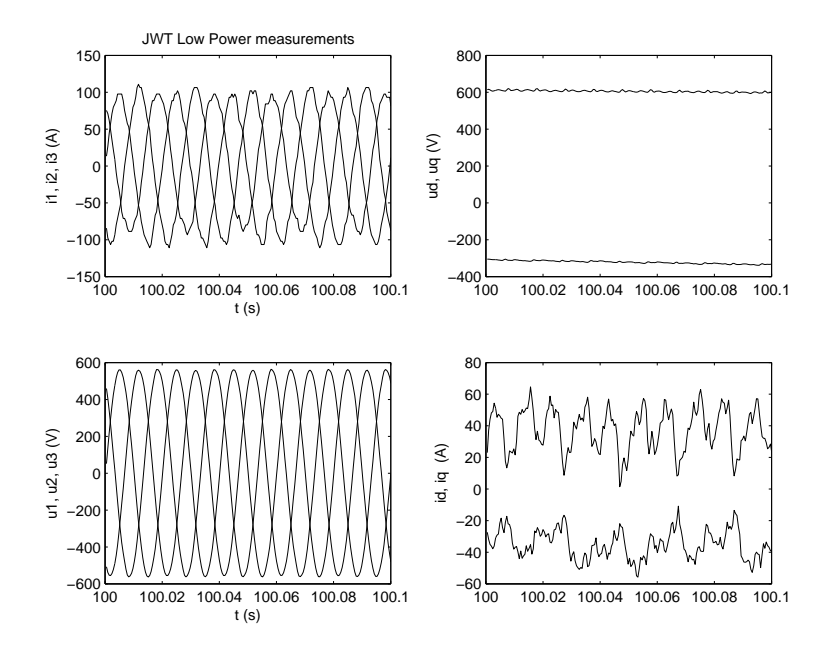


Figure 37: JWT turbine - Low Power - measurement: voltages and currents

Figure 38 shows the total active and reactive power  $P_{tot}$  and  $Q_{tot}$  and the active and reactive power of the grid side converter  $P_{cg}$  and  $Q_{cg}$ , calculated from the measured instantaneous grid phase voltages, the total currents and the grid side converter currents. The turbine produces about 80 kW and the converter power is 50 kW. Since the turbine speed is low, the converter power should be negative. This can be a definition problem. The APSD of measurements and simulation results will be compared, which eliminates a problem with the definition. The average reactive power of the converter and the total reactive power are small, about -8 kVA and about zero respectively.

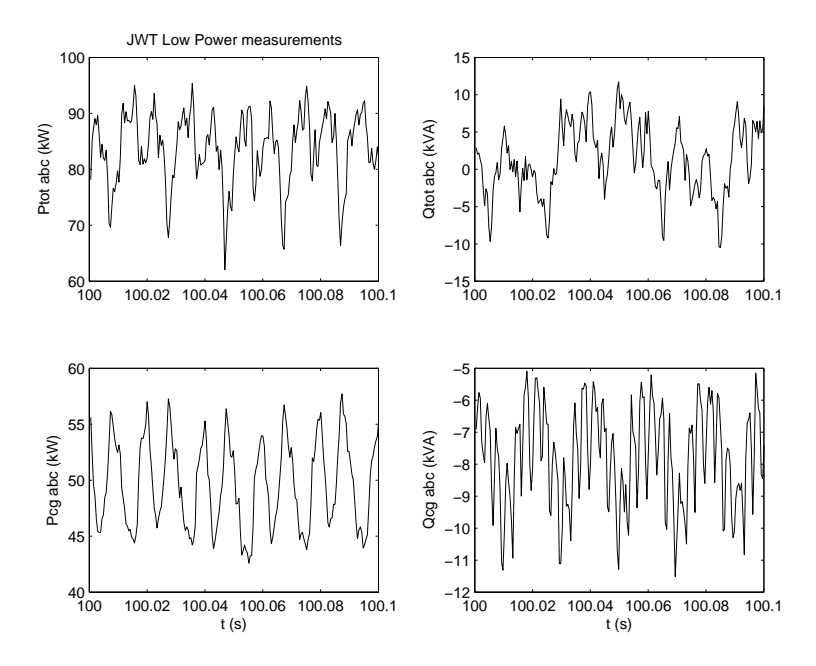


Figure 38: JWT turbine - Low Power - measurement: active and reactive powers

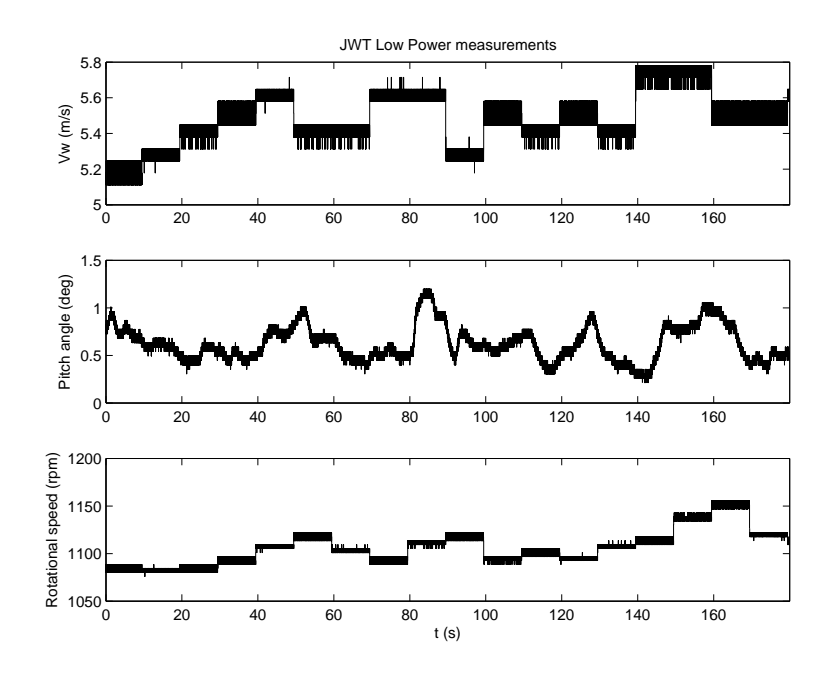


Figure 39: JWT turbine - Low Power - measurement: wind speed, pitch angle and rotational speed

Figure 39 shows the wind speed, pitch angle and rotational speed taken from the wind turbine data acquisition system. The speed is in the range of 1100-1150 rpm. The wind speed and rotational speed display step changes, which indicates a poor measurement. Only the average value of the wind speed will be input for the simulation.

# 5.9 Low power simulation

For the half power simulation the following choices have been made;

- the average single point wind speed is 5.4 m/s, the average value during the low power measurement;
- the input voltage is the moving average dq value of the measured instantaneous voltage (averaging time 10 ms) to exclude the high frequency harmonic noise. The voltage phasor angle is assumed to be constant;
- the choices concerning the model are equal to those for the full power simulation, see section 5.3.

The next five figures show the simulation results for the JWT turbine during low power normal operation. The high frequency noise on the electrical signals is caused by the noise on the input voltage  $v_{ds}$ , figure 42. The low frequency oscillations in the wind speed  $V_w E_{ff}$  and the areodynamic torque  $T_a$  are caused by tower passage and rotational sampling of the blades.

Figures 40 to 44 show a discontinuity at 120 s. At that time the rotor speed reached its lower limit and the mode of operation changes from variable speed to variable power. This increase the low frequency variability of a number of quantities, which include the active and reactive powers. Passing this limit in the power-speed control of the turbine will have an effect on the APSDs. The power-speed control of the JWT turbine may not react in the same way or may not be activated in the same way during the measurement.

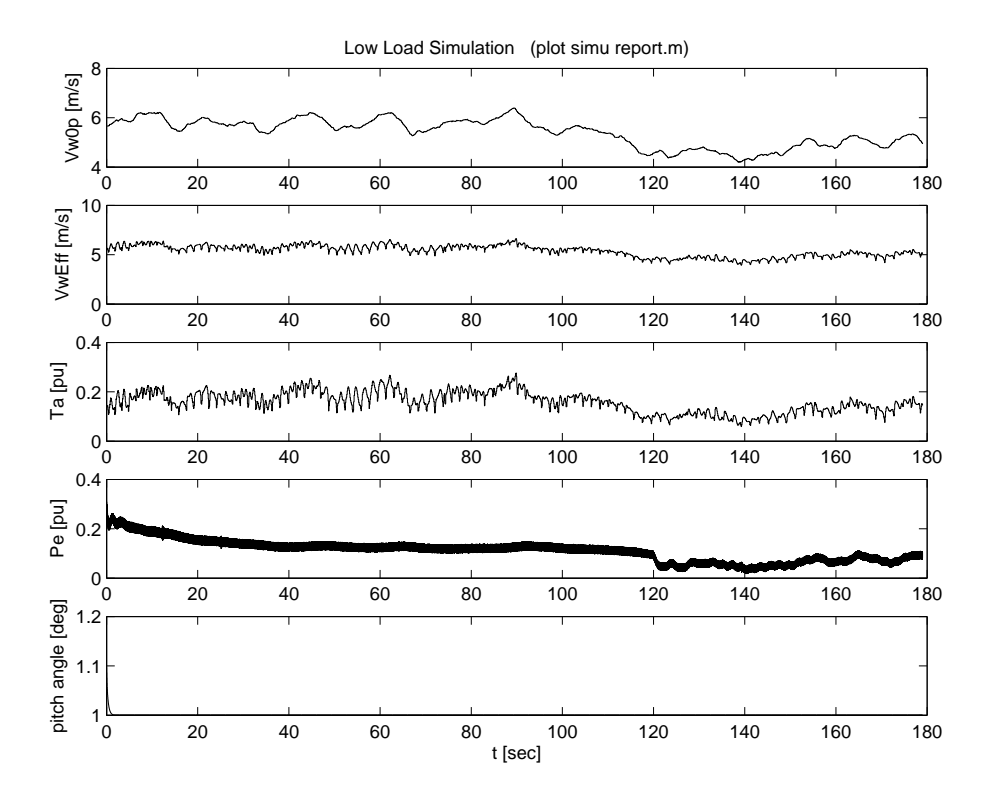


Figure 40: Low power - simulation: Rotor plane wind speed, rotor effective wind speed, aerodynamic torque, total electric power and pitch angle

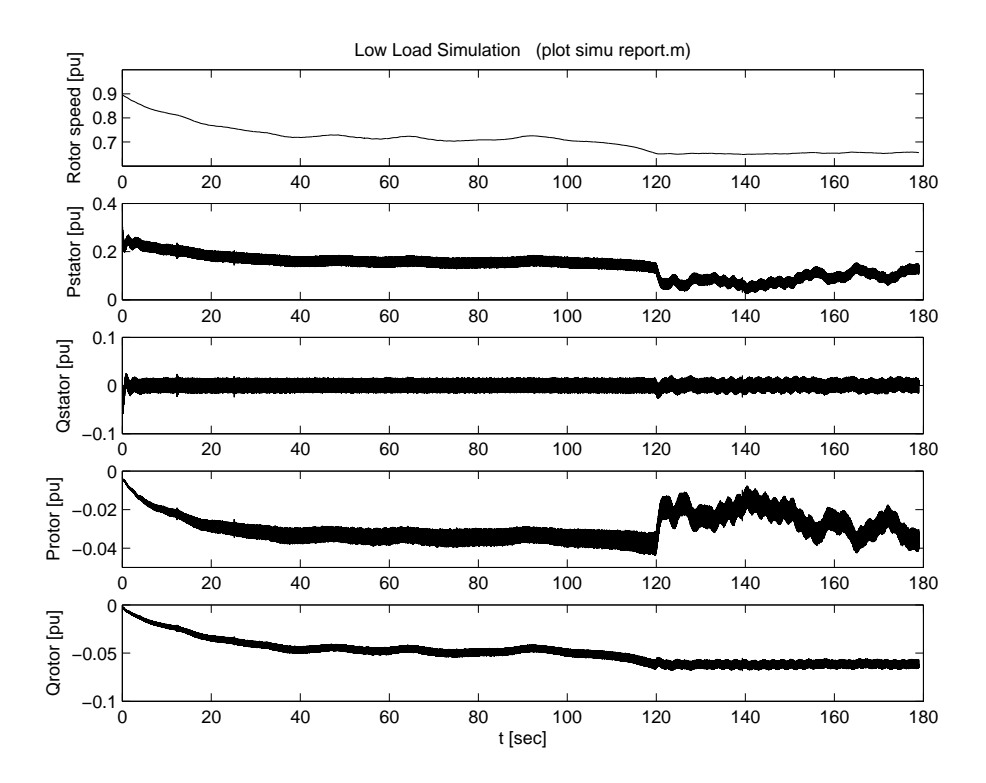


Figure 41: Low power - simulation: rotor speed, stator power, stator reactive power, rotor power and rotor reactive power

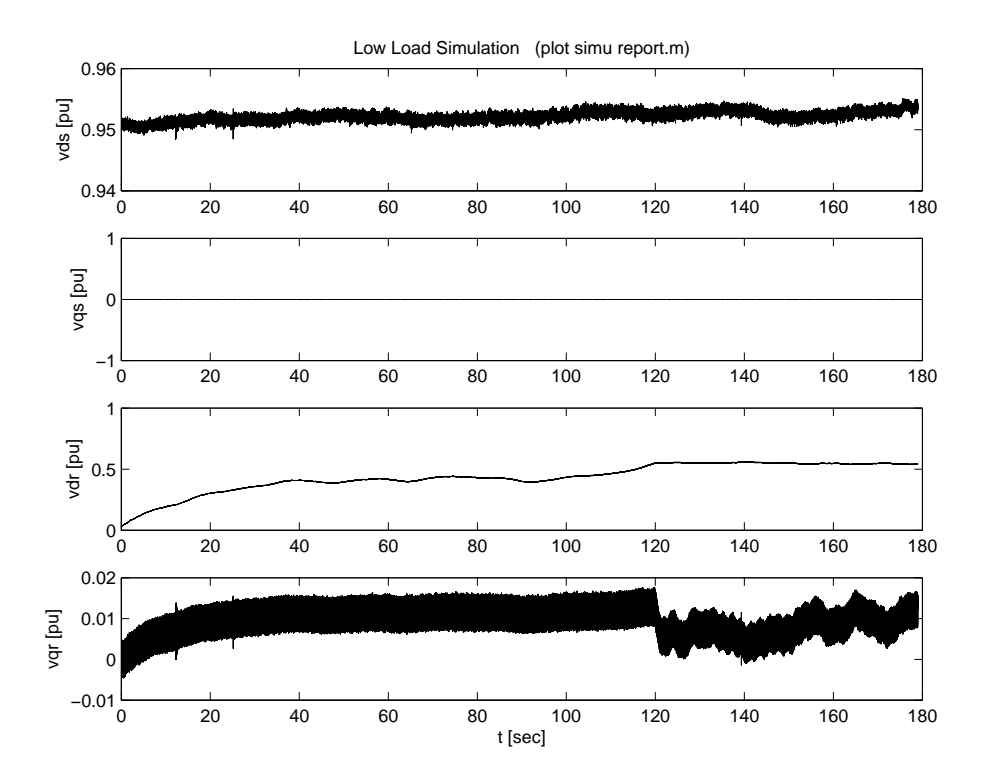


Figure 42: Low power - simulation: stator d- and q-voltage, rotor d- and q-voltage

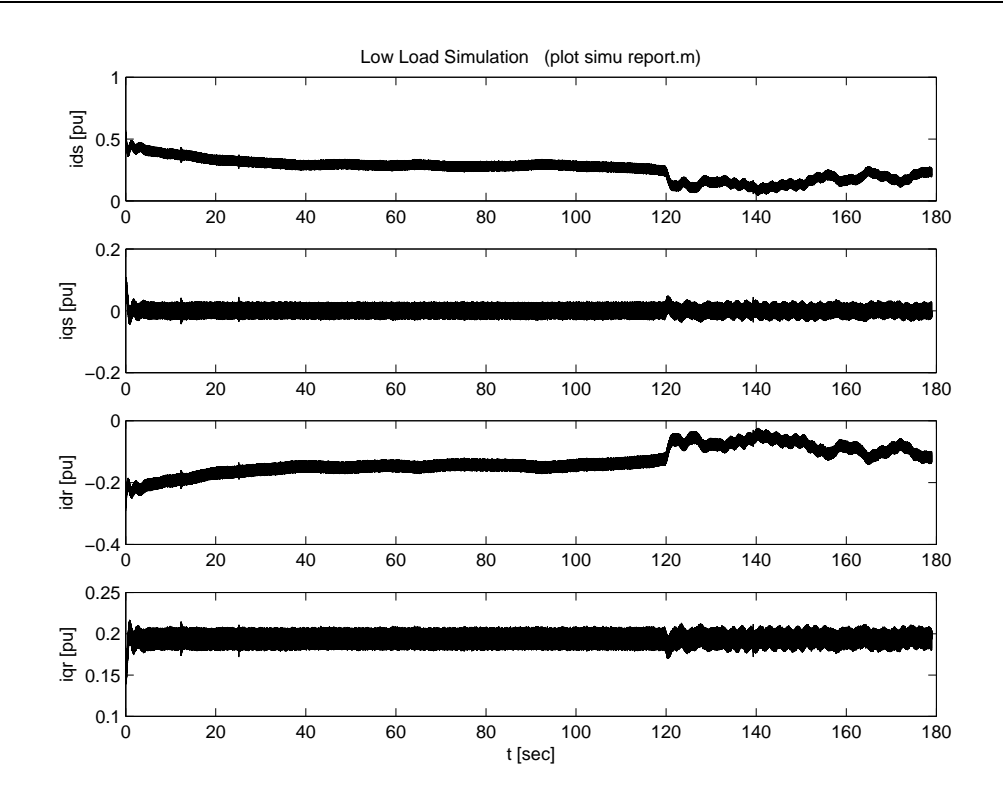


Figure 43: Low power - simulation: stator d- and q-current, rotor d- and q-current

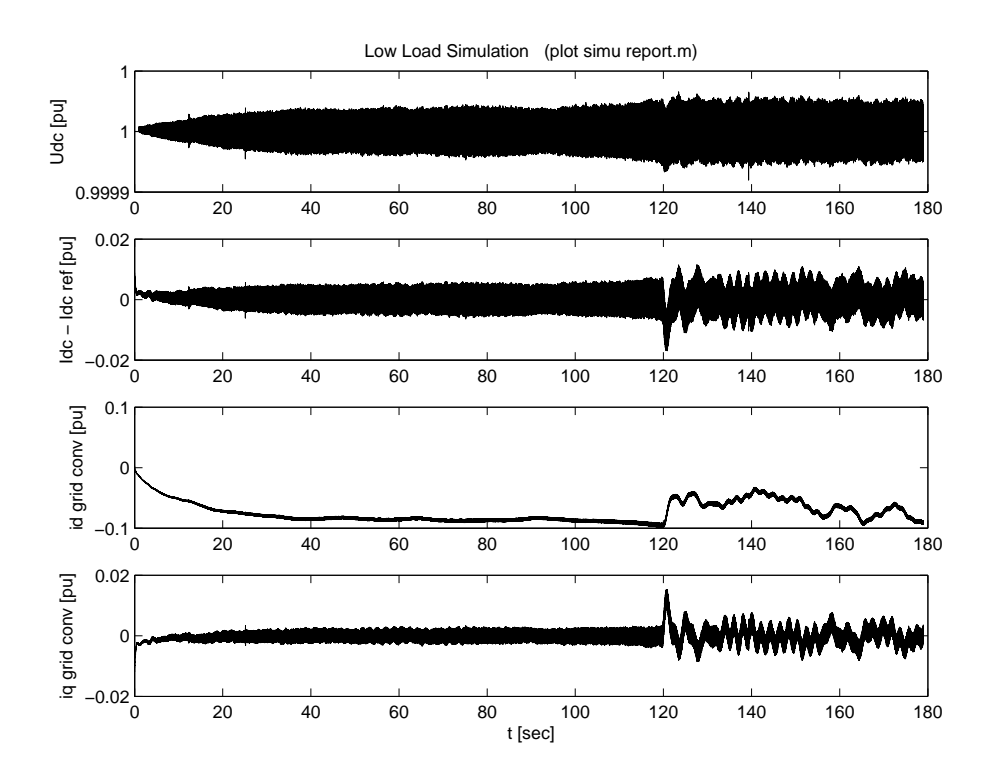


Figure 44: Low power - simulation: DC voltage deviation from setpoint, DC current deviation from setpoint, grid side converter d- and q-current

# 5.10 Comparing low power measurement and simulation results

Figures 45 to 47 compare the APSDs of the measured and simulated active powers for low power operation. The frequency content in the range of 1 to 60 Hz is similar for total and stator power. For the grid converter the simulated variability is a bit lower in this range. In the range of 0.1 to 1 Hz the differences between simulation and measurement for total and stator power are bigger, also when compared to the full and half power simulation.

The differences for the total and stator power in the low frequency range can be explained by hitting the lower speed limit in the simulation, which results in an increased variability of active power. The JWT turbine will have different power-speed settings and did not show a lower speed limit during the simulation (see figure 39).

Figures 48 to 50 compare the APSDs of the measured and simulated reactive powers for low power operation. The frequency content in the range of 1 to 60 Hz is similar. In the range of 0.1 to 1 Hz the differences between simulation and measurement are big, the reactive power is more variable in the simulation. This can be explained by a different reactive power controller design, as discussed in section 5.4.

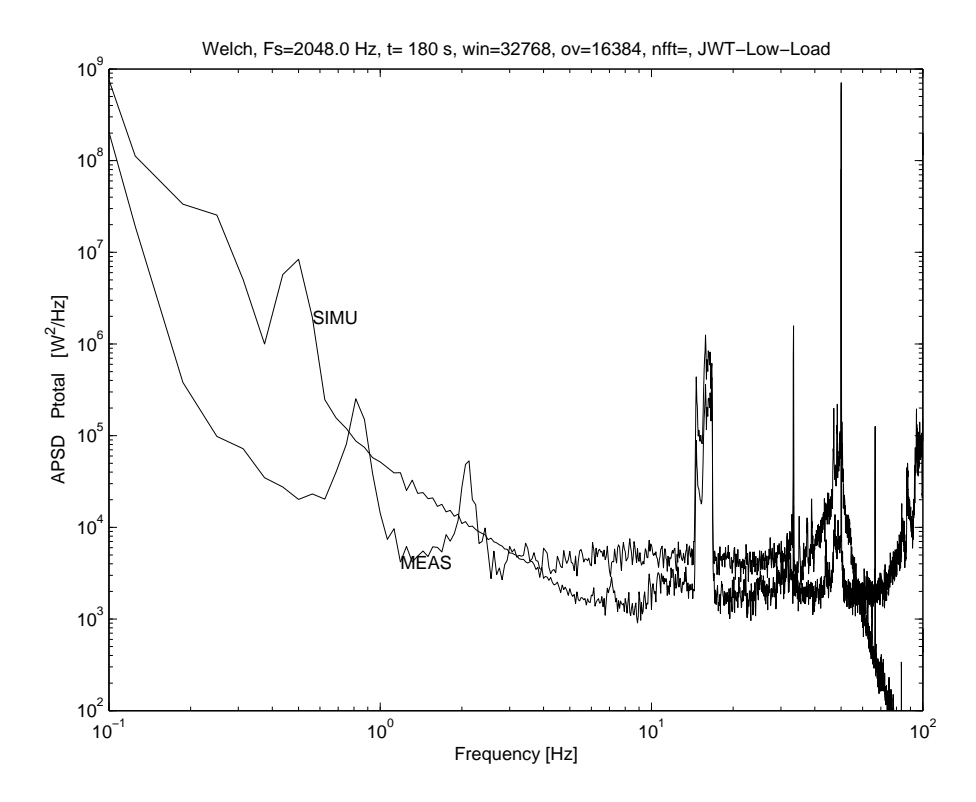


Figure 45: Low power - APSD: Total Power - measurement (MEAS) and simulation (SIMU)

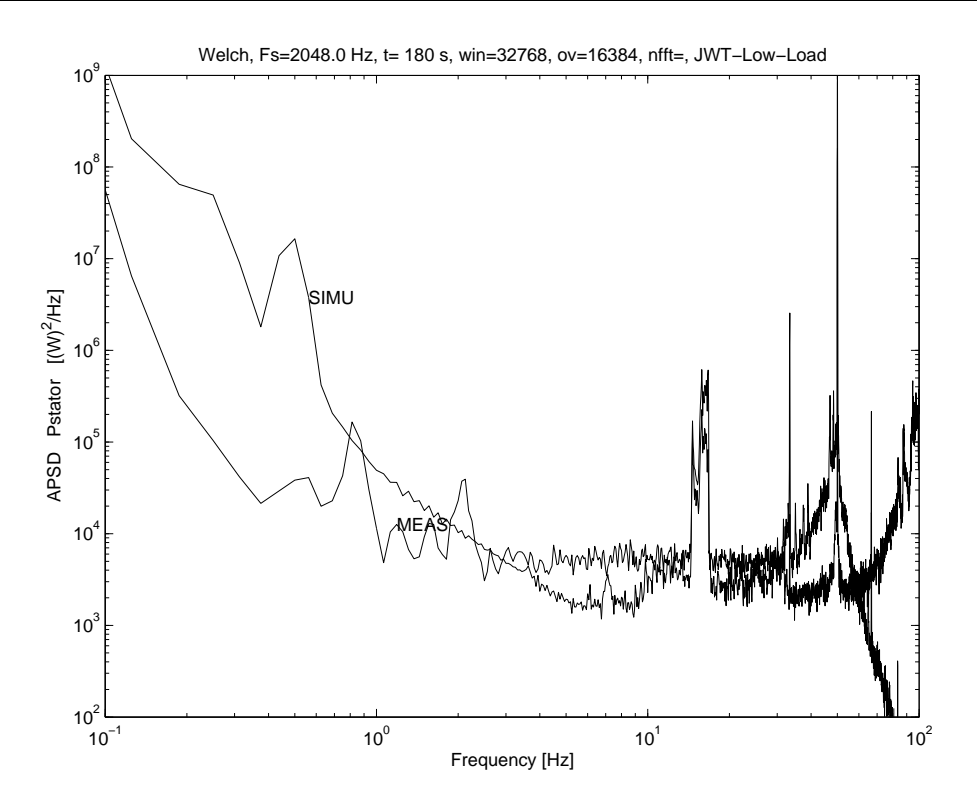


Figure 46: Low power - APSD: Stator Power - measurement (MEAS) and simulation (SIMU)

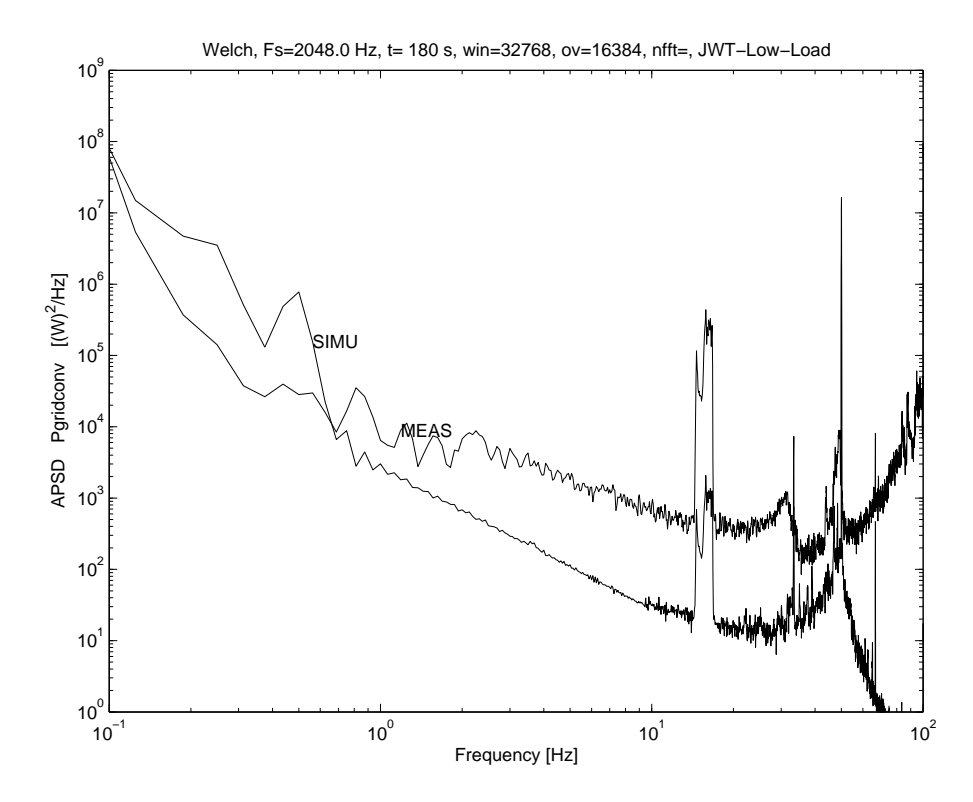


Figure 47: Low power - APSD: Grid side converter Power - measurement (MEAS) and simulation (SIMU)

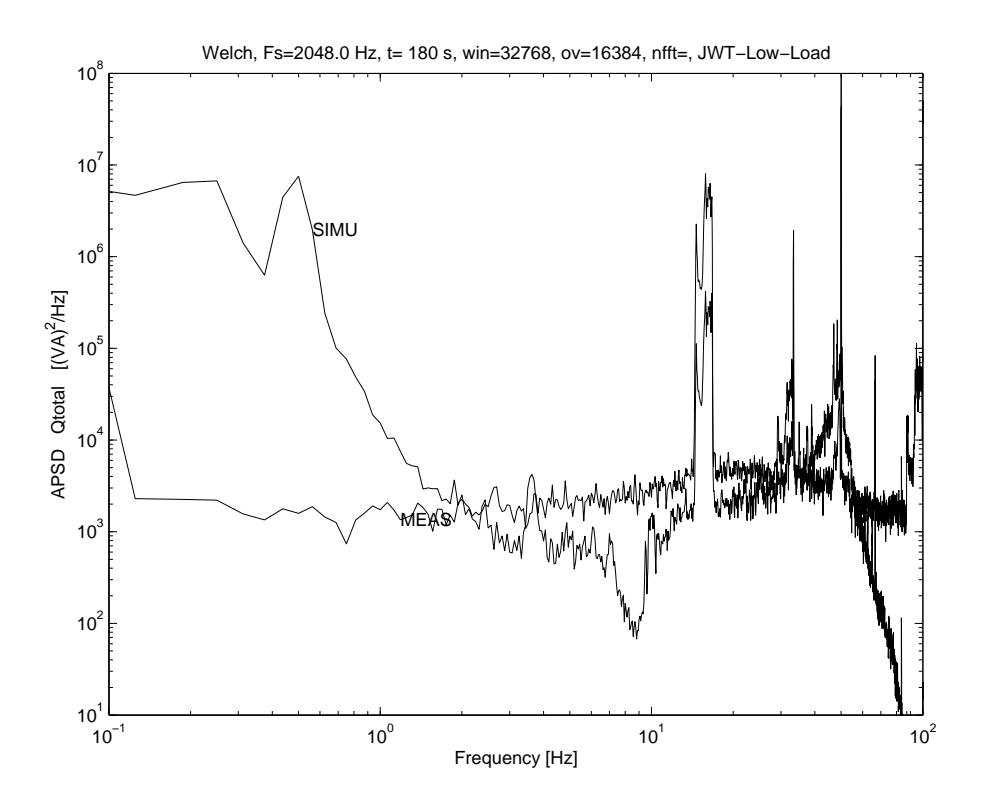


Figure 48: Low power - APSD: Total Reactive Power - measurement (MEAS) and simulation (SIMU)

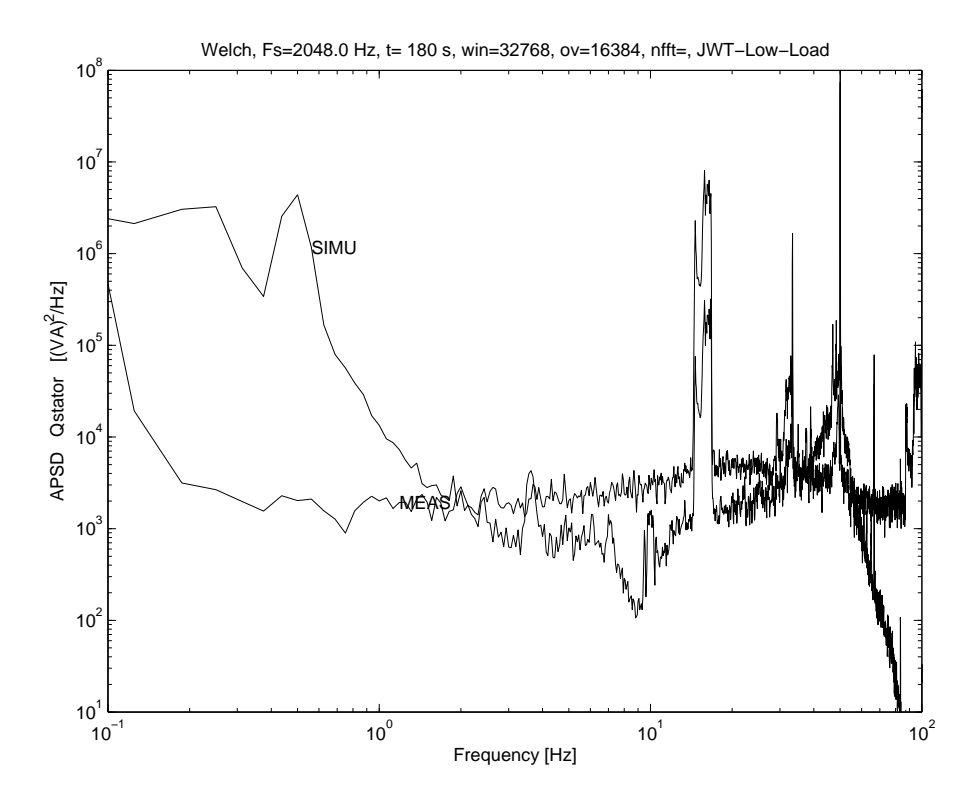


Figure 49: Low power - APSD: Stator Reactive Power - measurement (MEAS) and simulation (SIMU)

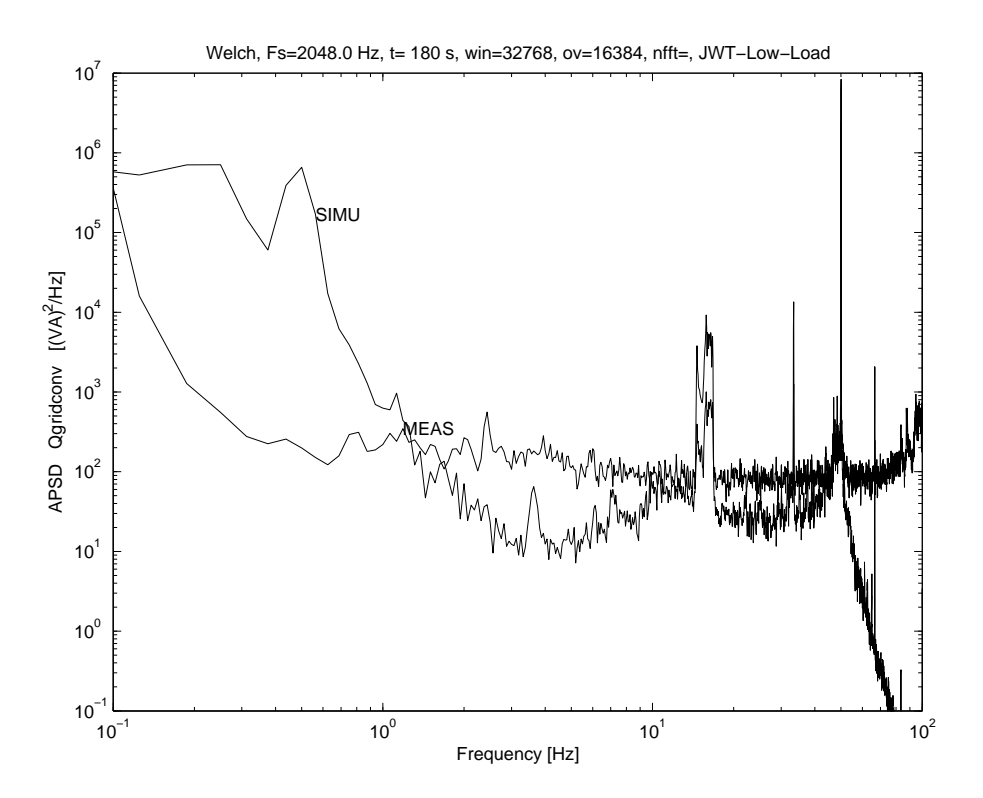


Figure 50: Low power - APSD: Grid side converter Reactive Power - measurement (MEAS) and simulation (SIMU)

# 5.11 Symmetrical voltage dip measurement

For the JWT turbine voltage dips measurement the three stator voltages and the three total currents (stator plus converter) have been recorded. The sample rate was 2048 Hz.

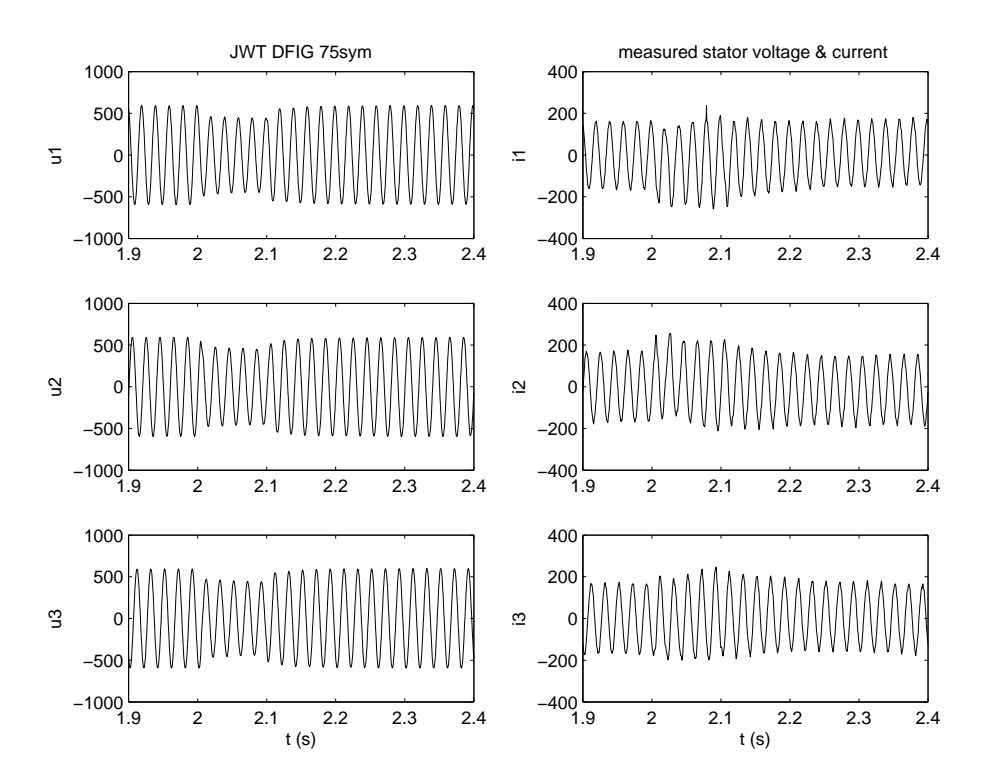


Figure 51: JWT turbine a voltage dip: measured three phase stator voltages and total currents

Figure 51 gives the measured instantaneous stator voltages and total currents during a voltage dip of 20-25%. The dip occurs in all three phases and was checked for asymmetry, which proved to be negligable (a few percent in voltage and current). Elimination of the unbalance, to make simulation and measurement results comparable, is therefore not needed.

A second aspect is the high frequency noise in the measurement caused by the switching of the converters (rotor side and grid side). The switching is not included in the model of the VSP-DFIG turbine: the converters are modelled by continously operating voltage sources. Therefore it makes sence to eliminate the high frequency noise from the measurements and use the filtered or averaged voltage as input for the simulation. Figure 52 compares the instantaneous voltage ( $\sqrt{u_d^2 + u_q^2}$ , with  $u_d$  and  $u_q$  the instantaneous stator voltage in the dq-reference frame) and the three phase moving average RMS voltage values for the measurement during the voltage dip:

$$u_{abc,rms} = \frac{1}{3N} \sqrt{\sum_{i=1:N} (u_{a,i}^2 + u_{b,i}^2 + u_{c,i}^2)}$$
 (1)

The averaging over half a period of the voltage oscillation (10 ms) eliminates the high frequency noise and reduced extreme values.

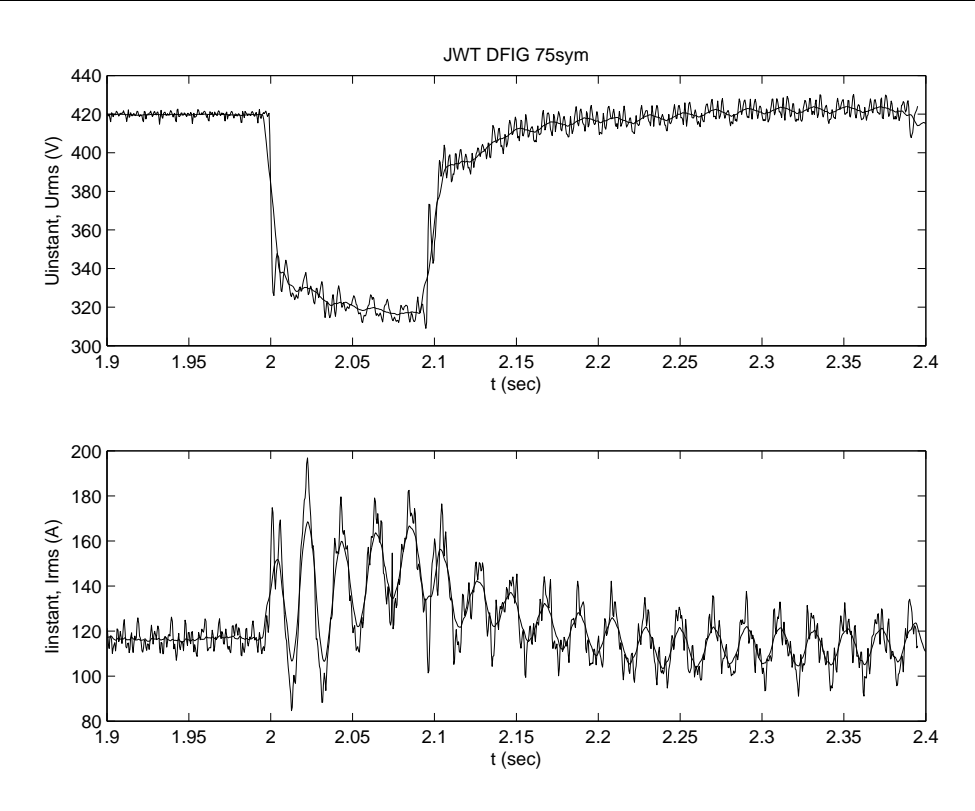


Figure 52: JWT turbine voltage dip: measured instantaneous and measured RMS moving average three phase voltage and total current

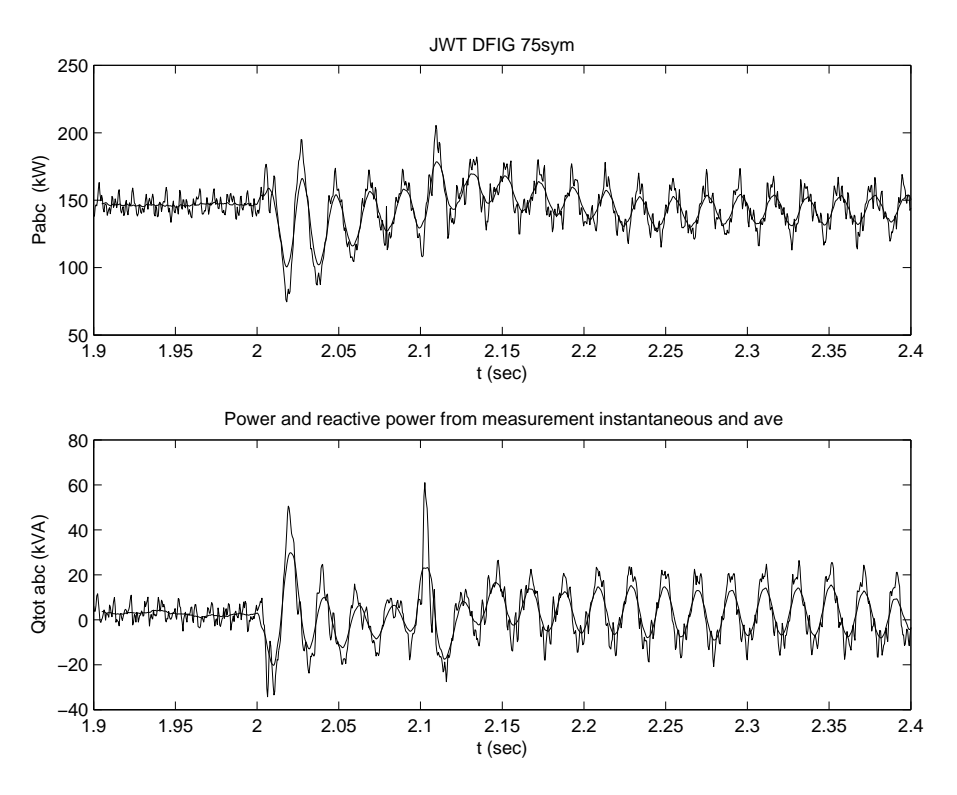


Figure 53: JWT turbine voltage dip: measured instantaneous and measured moving average three phase total power and total reactive power

Figure 53 compares the measured instantaneous and the average values of the total active power and total reactive power. The values are calculated as a moving average using a window of half the period of the voltage (0.01 sec):

$$P_{abc.inst} = u_a i_a + u_b i_b + u_c i_c (2)$$

$$P_{abc,ave} = \frac{1}{N} \sum_{i=1:N} P_{abc,inst,i}$$
 (3)

$$Q_{abc,inst} = (u_a(i_b - i_c) + u_b(i_c - i_a) + u_c(i_a - i_b))/\sqrt{3}$$
(4)

$$Q_{abc,inst} = (u_a(i_b - i_c) + u_b(i_c - i_a) + u_c(i_a - i_b))/\sqrt{3}$$

$$Q_{abc,ave} = \frac{1}{N} \sum_{i=1:N} Q_{abc,inst,i}$$
(5)

(6)

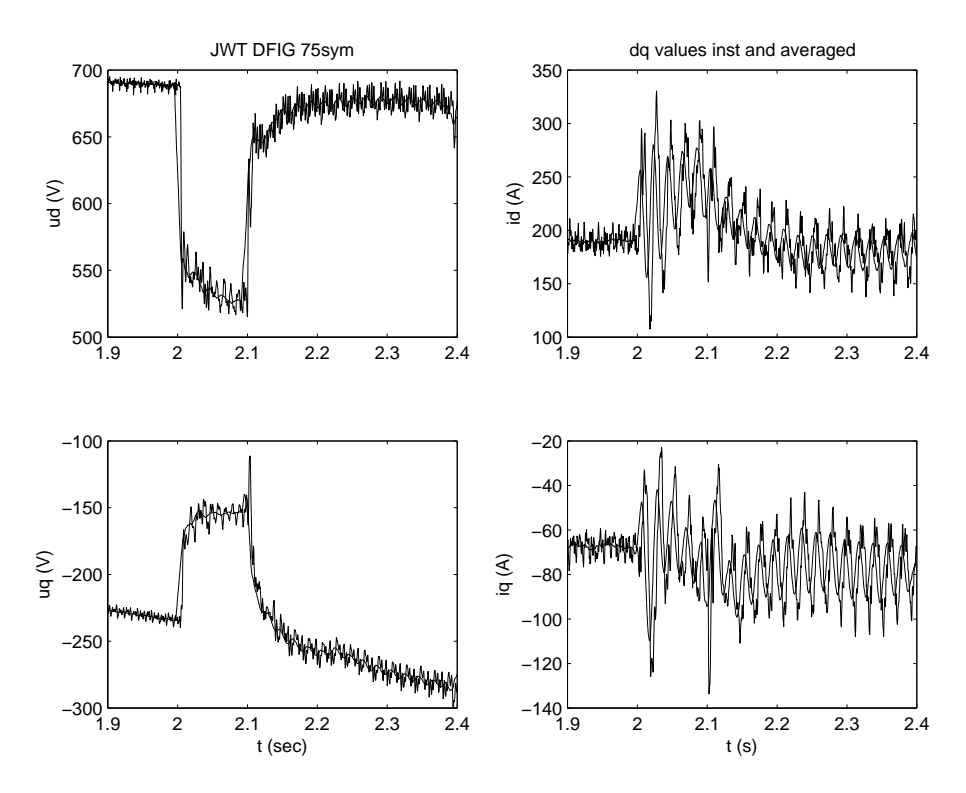


Figure 54: JWT turbine voltage dip: measured instantaneous dq and moving average dq stator voltage and current

Figure 54 gives the instantaneous and moving average dq-values of the stator voltage and total current calculated from the measured instantaneous phase voltage and total current values. Contrary to the simulations for the normal operation cases in the previous chapter, the voltage phasor rotational speed is assumed to be constant. The reason for this assumption is given in the Constant Speed Wind Farm validation report [5]. The dq-voltage values are input for the simulation and two simulation cases, instantaneous and moving average input voltage, will be compared. The moving average dq-values are similar to dq-values determined from RMS phase voltages. Voltage and current RMS values can not be used to calculate the dq-values since the information on the voltage phasor angle and the current phase angle is lost.

# 5.12 Voltage dip simulation

For the voltage dip simulation the following choices have been made;

- only the DFIG model was included in the simulation, since the response of the turbine rotor on a 10 ms time scale can be neglected (actually the rotor model is only updated every 10 ms);
- simulation results are compared for two sets of input voltages derived from measurement: instantaneous dq- and moving average dq-values.

The values are represented as per unit (pu) since the rated power of the simulated turbine and the JWT turbine differ. Figure 55 shows the instantaneous measured dq-voltages for the dip. Figure 56 compares the measured and simulated total active and total reactive power for the instantaneous measured dq-voltages as input. Since the model does not include switching of the IGBTs, the simulation is less noisy. The simulation is somewhat out of phase with the measurement and is less damped. Differences in parameters can easily cause these effects. From a general perspective, measurement and simulation are similar.

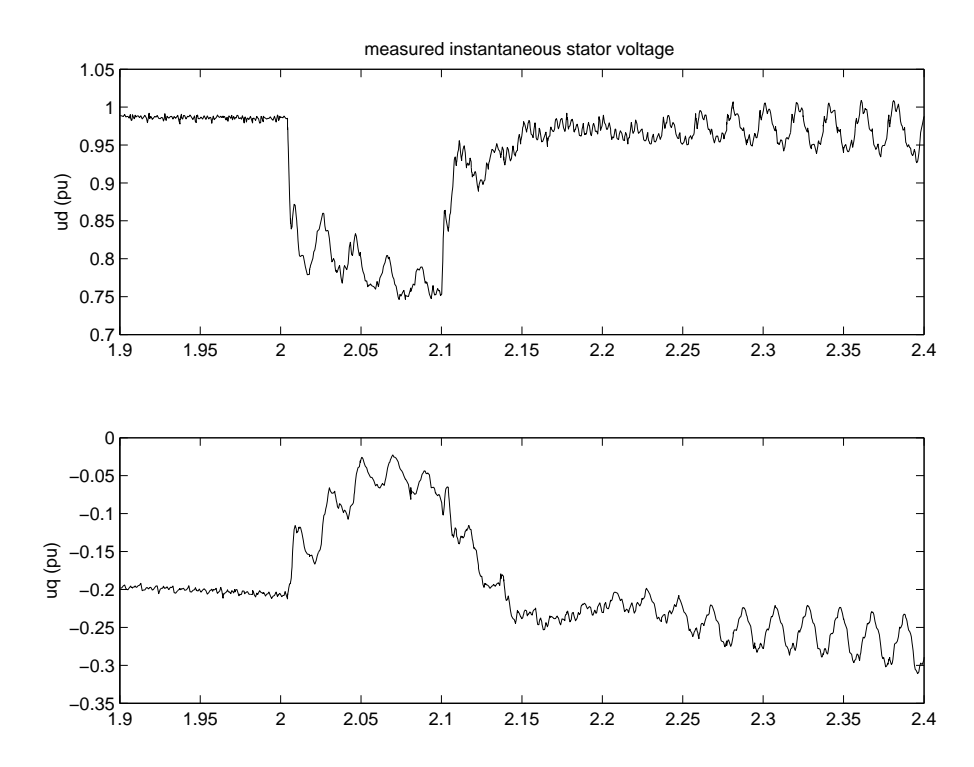


Figure 55: JWT turbine voltage dip: measured instantaneous dq input voltage

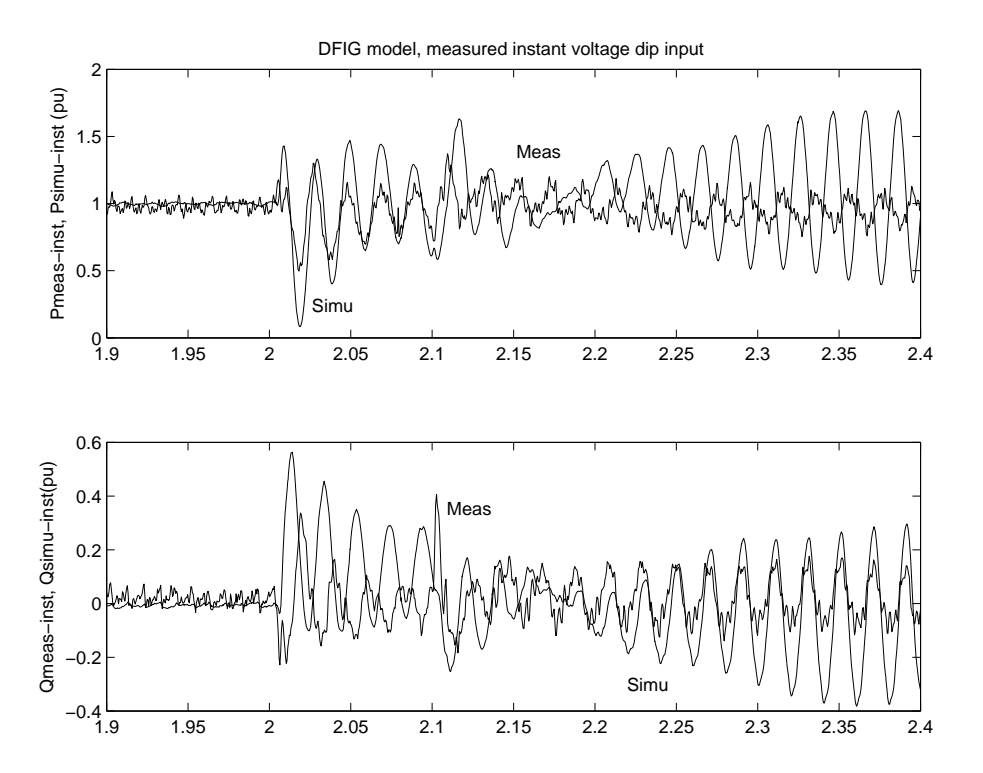


Figure 56: JWT turbine voltage dip: measured and simulated total active and total reactive power (measured instantaneous dq input voltage)

Figure 57 shows the averaged measured voltages for the dip. Figure 58 compares the measured and simulated total active and total reactive power for the measured averaged dq-voltage as input. Due to the averaging, the high frequency noise disappeared from the measurement. The differences are similar to the simulation with instantaneous dq-voltage input.

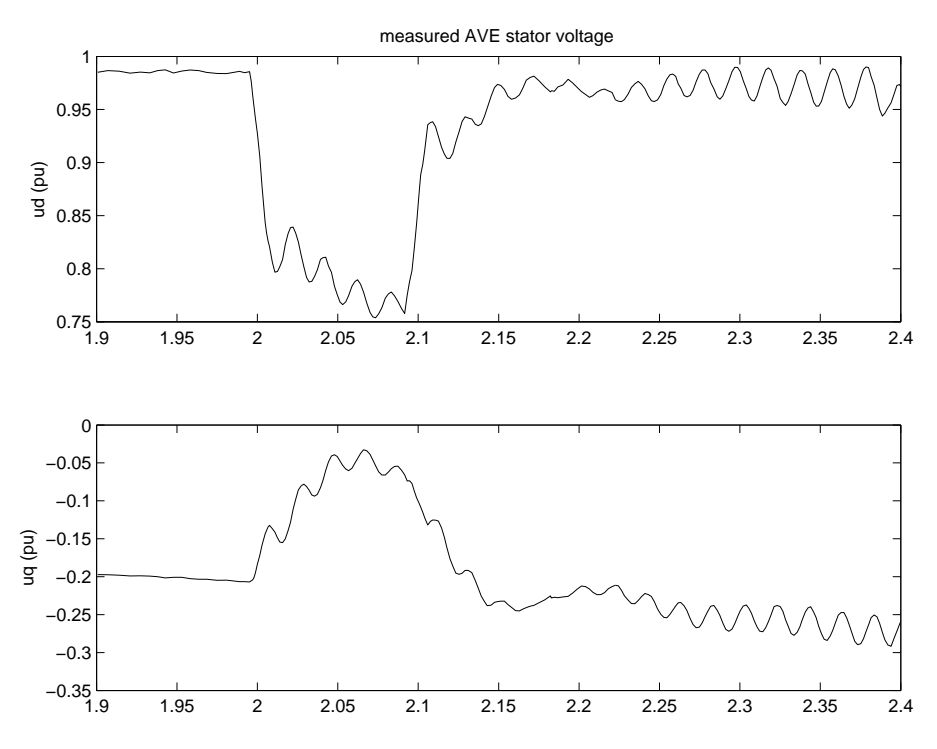


Figure 57: JWT turbine voltage dip: measured average dq input voltage

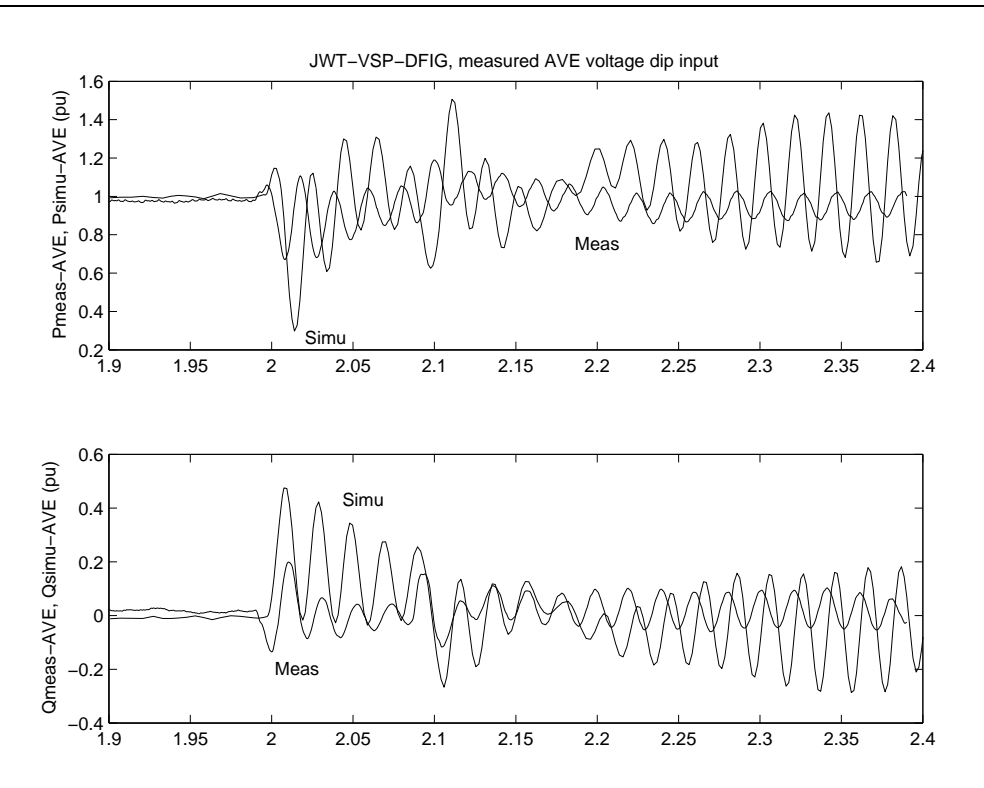


Figure 58: JWT turbine voltage dip: measured and simulated total active and total reactive power (measured average dq input voltage)

# 6 CONCLUSIONS AND RECOMMENDATIONS

For a successful validation of dynamic models of wind turbines and wind farms, which include the electrical system and its control, the requirements on the measurements and turbine data to be used for validation are high:

- detailed information on the turbine design and parameters is required, especially regarding the controller design (pitch controller as well as the electrical controllers);
- the measurement should have a high sample rate and adequate anti-aliasing filtering;
- preferably simultaneous measurement of mechanical as well as electrical variables;
- the wind turbine should preferably be a representative, commercial turbine.

None of the sets of measurement on variable speed turbines available in the IEA Annex XXI satisfied all (or even most) of these requirements. The CART turbine in the data base included detailed turbine information but was not a commercial turbine and therefore not representative. The JWT turbine is a commercial turbine but lacked detailed information on turbine parameters and did not include mechanical measurements. The IEA Annex XXI working group decided that the JWT turbine presented the best choice, even though detailed turbine data is missing. For the time being, a better option was not available. The lack of turbine parameters for the JWT turbine limits the scope of this model validation, however.

#### 6.1 Discussion of the validation results

Part of the Erao-2 model library has been validated by comparing measurements of the variable speed JWT turbine to simulations with the variable speed wind turbine model with doubly fed induction generator in the model library. The validation covered three cases of normal operation and a voltage dip.

For normal operation the power spectral density of the active and reactive power at the measurement locations (grid side converter and total) have been compared. From a general perspective, the APSDs of measurements and simulations were similar but the details were often different. This is not surprising since detailed knowledge on the JWT turbine parameters and control was missing. From the results for normal operation the following observation can be made:

- The spectra for the active powers showed a better match than for the reactive powers. The power control follows the wind power and if the wind input and the power control are modelled correctly, this will result in a good representation of the active power, unless the voltage spectrum in the measurement is different from that in the simulation, which is not the case since the measured voltage was input for the simulations.
- The differences between the spectra of the measured and simulated reactive powers can be explained by differences in the reactive power controller design, which consists of two separate designs, one for the stator reactive power via the rotor current and one for the grid converter reactive power via the converter current. Since the details of the JWT turbine controller designs were not known, commonly used designs were chosen. A different design can easily lead to the observed differences in behaviour.
- Peaks occuring at specific frequencies in the measurement were not reproduced in the simulations. This is no surprise, since the validation was limited by the missing turbine data. As mentioned before, this is the major drawback of this validation.

52 ECN-E-07-008

Form the comparison of the voltage dip measurements and simulations a similar conclusion can be drawn. The oscillation frequency in measurement and simulation was similar, but the oscillation was more extreme in the simulation and the damping was less. The differences between simulation and measurement are attributed to differences in parameter values. From a general perspective, measurements and simulation results for the voltage dip are not that far apart, however.

#### 6.2 Conclusion

Due to the limitations discussed in the previous sections, detailed conclusions on the accuracy of the VSP-DFIG model can not be drawn from the validation based on the JWT turbine measurements. Nevertheless, the validation results showed that, even if most of the turbine parameters are not known, the dynamic simulation produces results which are not that different from the measurements. This is a useful conclusion, since detailed information on commercial turbines is often missing. On the other hand, the validation did not lead to suggestions for model improvement, since the model could only be validated in a global way.

#### 6.3 Recommendation

It is recommended to execute additional validation exercises when a suitable sets of VSP turbine measurements and turbine data are available.

54 ECN-E-07-008

# REFERENCES

- [1] Kleinrath H. *Stromrichtergespeiste Drehfeldmachinen*. Springer Verlag, Wien , New York, 1980. p. 197.
- [2] Waldo V. Lyon. Transient analysis of alternating-current machinery: an application of the method of symmetrical components. MIT and John Wiley & Sons, Inc., New York, 1954.
- [3] J.T.G. Pierik. CSS Wind Farm Dynamic Model Validation: Alsvik measurements and simulations. Technical Report ECN-C-xxx, ECN, 2005.
- [4] J.T.G. Pierik, M.E.C. Damen, P. Bauer, and S.W.H. Electrical and control aspects of offshore wind farms, Phase 1: Steady state electrical design and economic modeling, Vol. 1: Project results. Technical Report ECN-CX-01-083, ECN Wind Energy, 2001.
- [5] J.T.G. Pierik and J. Morren. Constant Speed Wind Farm Dynamic Model Validation; Alsvik measurements and simulations. Technical Report ECN-E-07-007, ECN, 2007.
- [6] J.T.G. Pierik and J. Morren. Validation of dynamic models of wind farms (Erao-3): Executive summary, benchmark results and model improvements. Technical Report ECN-E-07-006, ECN, 2007.
- [7] J.T.G. Pierik, J. Morren, E.J. Wiggelinkhuizen, S.H.W. de Haan, T.G. van Engelen, and J. Bozelie. *Electrical and Control Aspects of Offshore Wind Turbines II (Erao-2). Volume 1: Dynamic models of wind farms*. Technical Report ECN-C--04-050, ECN, 2004. available at the web site of ECN (*www.ecn.nl*, use search option).
- [8] J.T.G. Pierik, J. Morren, E.J. Wiggelinkhuizen, S.H.W. de Haan, T.G. van Engelen, and J. Bozelie. *Electrical and Control Aspects of Offshore Wind Turbines II (Erao-2). Volume 2: Offshore wind farm case studies*. Technical Report ECN-C- -04-051, ECN, 2004. available at the web site of ECN (*www.ecn.nl*, use search option).
- [9] J.O.G. Tande and et. al. Benchmark test of dynamic wind generation models for power system studies. IEEE Trans PWRS, Special Section on Power System Performance Issues Associated with Wind Energy, 2006.
- [10] T. Thiringer and A. Petersson. *Control of a variable-speed pitch-regulated wind turbine*. Technical report, *Chalmers University of Technology*, 2005.

ECN-E-07-008 55

# A MODEL IMPROVEMENT

During the validation of the VSP-DFIG turbine model two problems occurred. The first was a result of assumptions in the controller design and the second was caused by unsufficient filtering of noise.

# DFIG controller operating on rotating voltage phasors

In the simulation of normal operation at full power a problem occured when the measured voltages were converted to d- and q-axis under the assumption of constant phasor rotational speed (equivalent to constant frequency). If these dq-values were used as input for the VSP-DFIG turbine model, the model was unstable. The DFIG controller in the model can not work if the voltage phasor rotates 360 degrees, which was the case for the dq-phasor calculated from the measured voltages. The reason for this problem is that the design of the controller assumes that a voltage reference frame in the direction of  $v_{qs}$ , so  $v_{ds} = 0$  [7]. As long as the value of  $v_{ds}$  is relatively small and  $v_{qs}$  remains positive, the controller works fine. In general, the d- and q-axis voltages can be chosen to satisfy this requirement by a coordinate transformation. The problem was solved by redefining the voltage reference, e.g. align the measured space phasor voltage to the q-axis. This is equivalent to a different transformation between the voltage phasor of the grid and the voltage phasor of the generator. This method is also used when a number of synchronous machines, with instantaneous differences in rotational speed, operate on the same AC grid. The choice works fine for slow changes but may causes problems during a fast change like a voltage dip, when a sudden change in voltage phasor angle plays an important role.

#### High frequency noise in the measured voltage

A second problem that occured in the simulation of normal operation at full power was caused by the high frequency noise in the measured voltage. Variations of about three percent in the measured voltage caused variations in the DFIG electric power at full load of about 27%. This is considerably higher than in the measurements, where a high frequency power variation of 10% is seen. There can be several reasons for the difference between measurement and simulation:

- 1. the voltage variation can be amplified by one of the control loops of the electrical system;
- 2. the parameters of the model are not representative for the measured system.

Amplification by one of the control loops can be prevented by filtering the controller inputs. Introducing a third order Butterworth filter with a cut-off frequency of 10 Hz in the master controllers of the torque and reactive power control loops of the DFIG did not have a significant effect. In the third control loop on the DC link voltage, the variation in this voltage is small 0.1 V per 1000 V, so this controller is not expected to cause the power oscillation. This premise was tested by switching the controller of temporarily, which did not reduce the power oscillations.

So the cause appears to be the parameter values of the transformer and the DFIG generator. The parameters of the DFIG and the three winding transformer have been chosen according to manufacturer specifications. The parameters correspond to an existing VSP-DFIG system but not to the system that was measured, since the JWT VSP-DFIG parameters were not available. To find the parameters which influence the power oscillation, the transformer dynamics was eliminated from the model. This increased the oscillation of the power to 54%. Increasing the transformer resistance by a factor 4 decreases power oscillation by a factor 2. If the stator resistance of the induction generator is increased by a factor two the same reduction in power oscillation occurs.

56 ECN-E-07-008

# B CALCULATION OF POSITIVE SEQUENCE, FUNDAMEN-TAL HARMONIC AND RMS VALUES

### **B.1** Steady-state conditions

The method of symmetrical components (in phase or zero sequence, normal or positive sequence and reverse or negative sequence component) was originally developed by Fortescue in 1918 for the purpose of analyzing the steady-state performance of rotating electrical machines under unbalanced (asymmetrical) conditions. In this method the phasors (vectors rotating at a given, not necessary constant speed) that represent the voltages and currents in the phases of an unbalanced system are resolved in their symmetrical components. If the electrical system is in a steady-state condition, the phasors are constant.

If the time phasor of alternating voltage  $v(t) = \hat{V}\cos(\omega t + \alpha) = \operatorname{Re}(\hat{V}\mathrm{e}^{\mathrm{j}(\omega t + \alpha)})$  is  $\vec{V} = \hat{V}\mathrm{e}^{\mathrm{j}\alpha}$ , both  $\hat{V}$  and  $\alpha$  are constant in steady state. If  $\vec{V}_a, \vec{V}_b$  and  $\vec{V}_c$  are the phasors of the three phase alternating voltages of a three phase system, the instantaneous zero, positive and negative sequence components of  $\vec{V}_a$  then are:

$$\vec{V}_{a0} = \frac{1}{3}(\vec{V}_a + \vec{V}_b + \vec{V}_c) \tag{7}$$

$$\vec{V}_{a1} = \frac{1}{3}(\vec{V}_a + z \cdot \vec{V}_b + z^2 \cdot \vec{V}_c) \tag{8}$$

$$\vec{V}_{a2} = \frac{1}{3}(\vec{V}_a + z^2 \cdot \vec{V}_b + z \cdot \vec{V}_c) \tag{9}$$

and

$$\vec{V}_{b0} = \vec{V}_{a0}$$
 (10)

$$\vec{V}_{b1} = z^2 \vec{V}_{a1} \tag{11}$$

$$\vec{V}_{b2} = z\vec{V}_{a2} \tag{12}$$

$$\vec{V}_{c0} = \vec{V}_{a0}$$
 (13)

$$\vec{V}_{c1} = z\vec{V}_{a1} \tag{14}$$

$$\vec{V}_{c2} = z^2 \vec{V}_{a2} \tag{15}$$

with  $z=\exp 2\pi j/3$  and  $z^2=\exp 4\pi j/3$ . So the amplitudes of the positive sequence phasors are equal (indicating balanced conditions) and the same is true for the amplitudes of the negative and zero sequence phasors respectively. These sets symmetrical components then replace the actual voltages and currents in the Kirchhoff equations that represent the electrical system. The values of the phase voltages in terms of the symmetrical components of  $\vec{V}_a$  are:

$$\vec{V}_{a} = \vec{V}_{a0} + \vec{V}_{a1} + \vec{V}_{a2} \tag{16}$$

$$= \vec{V}_{b0} + z \cdot \vec{V}_{b1} + z^2 \cdot \vec{V}_{b2} \tag{17}$$

$$= \vec{V}_{c0} + z^2 \cdot \vec{V}_{c1} + z \cdot \vec{V}_{c2} \tag{18}$$

$$\vec{V}_b = \vec{V}_{a0} + z^2 \cdot \vec{V}_{a1} + z \cdot \vec{V}_{a2} \tag{19}$$

$$= \vec{V}_{b0} + \vec{V}_{b1} + \vec{V}_{b2} \tag{20}$$

$$= \vec{V}_{c0} + \vec{V}_{c1} + \vec{V}_{b2}$$

$$= \vec{V}_{c0} + z \cdot \vec{V}_{c1} + z^2 \cdot \vec{V}_{c2}$$
(21)

ECN-E-07-008 57

$$\vec{V}_c = \vec{V}_{a0} + z \cdot \vec{V}_{a1} + z^2 \cdot \vec{V}_{a2} \tag{22}$$

$$= \vec{V}_{b0} + z^2 \cdot \vec{V}_{b1} + z \cdot \vec{V}_{b2} \tag{23}$$

$$= \vec{V}_{c0} + \vec{V}_{c1} + \vec{V}_{c2} \tag{24}$$

Positive and negative sequence abc-phasors are 120 degrees out of phase, while the b and c phase have switched places. The zero sequence abc-phasors do not have an angle difference. The set of a-phasors can be added vectorially to generate the actual (unbalanced) a-phasor, see figure 59.

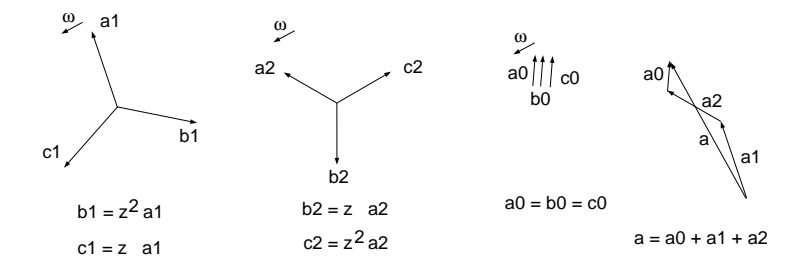


Figure 59: Graphical representation of three phase time phasors by symmetrical component decomposition

#### **B.2** Non steady-state conditions

The method of symmetrical components has mostly been applied to steady state conditions but can be applied to represent the dynamic operation of electrical machines as well [2]. Two options are:

- use the same phasor method as for steady-state  $\vec{V}=\hat{V}\mathrm{e}^{\mathrm{j}\alpha}$ , but now both  $\hat{V}$  and  $\alpha$  are variable. This makes associating these with RMS or peak values a bit tricky;
- apply the Fortescue transformation to the instantaneous phase values in stead of to phasors.

For the second option, since the instantaneous values are real, the phasors which represent the positive and negative sequence values are generally complex. If  $v_a, v_b$  and  $v_c$  are the instantaneous values of the three phase voltages of a three phase system, the instantaneous zero, positive and negative sequence components of  $v_a$  are:

$$v_{a0} = \frac{1}{3}(v_a + v_b + v_c) \tag{25}$$

$$v_{a0} = \frac{1}{3}(v_a + v_b + v_c)$$

$$v_{a1} = \frac{1}{3}(v_a + z \cdot v_b + z^2 \cdot v_c)$$

$$v_{a2} = \frac{1}{3}(v_a + z^2 \cdot v_b + z \cdot v_c)$$
(25)
(26)

$$v_{a2} = \frac{1}{3}(v_a + z^2 \cdot v_b + z \cdot v_c) \tag{27}$$

For the zero, positive and negative sequence components of  $v_b$  and  $v_c$  similar relations hold as in case of phasor quantities.

Phasors in alternating current electrical machines may have two meanings:

- they may represent an in time sinusoidally changing quantity (time phasors). Time phasors are complex, and are also applicable for other electrical component which do not have a rotating electromagnetic field;
- or they may represent the combined vectorial (spacial) sum of a magnetic field, current or voltage distribution in three distributed windings of an AC electrical machine. The direction for each individual winding (or phase) vector is the axis of the distributed winding. The vectorial sum results in a space vector rotating with respect to the individual windings and is often called a space phasor. This is a different type of quantity than the time phasor. In a three phase winding system with 120 degrees distributed windings and voltages and currents which are 120 degrees out of phase in time as well, the result is a space phasor which is rotating with a variable speed.

The sequence components of a stationary winding (non-rotating but not in steady state operation) are two counter-rotating vectors of equal size plus a constant non-rotating vector in the direction of the winding. The instantaneous real value of a winding quantity can be represented by the vectorial sum of the sequence components. The real axis is in the direction of the winding axis. The two counterrotating vectors are equivalent to two complex conjugated numbers, the positive and negative sequence value. The vectorial sum of these three components will always be in the direction of the winding axis.

Adding the positive sequence component of the three windings produces a rotating quantity in positive direction (also if the winding itself is stationary). Secondly, the negative sequence components of all three phases will give a rotating quantity in negative direction. The three constant phase components will not give a rotating quantity if they have equal value, which is the case.

The values of the instantaneous phase voltages in terms of symmetrical components of  $v_a$  are:

$$v_a = v_{a0} + v_{a1} + v_{a2} (28)$$

$$v_b = v_{b0} + v_{b1} + v_{b2} (29)$$

$$= v_{a0} + z^2 \cdot v_{a1} + z \cdot v_{a2} \tag{30}$$

$$v_c = v_{c0} + v_{c1} + v_{c2} (31)$$

$$= v_{a0} + z \cdot v_{a1} + z^2 \cdot v_{a2} \tag{32}$$

The positive sequence components of  $v_a, v_b$  and  $v_c$  are  $v_{a1}, z^2 \cdot v_{a1}$  and  $z \cdot v_{a1}$  respectively. The negative sequence components of  $v_a, v_b$  and  $v_c$  are  $v_{a2}, z \cdot v_{a2}$  and  $z^2 \cdot v_{a2}$  respectively. All phase voltages have the same zero sequence component, viz.  $v_{a0}$ . Since the phase voltages are real quantities and since z and  $z^2$  are complex conjugate values, the positive sequence component  $v_{a1}$  and the negative sequence component  $v_{a2}$  are alway complex conjugate values:  $v_{a2} = \operatorname{conj}(v_{a1})$ . The zero sequence component is alway real. Similar relations hold for the phase currents.

Some observations can be made:

- the Fortesque transformation, if applied to instantaneous values, transforms the complete frequency content of the original signal, so higher harmonic component are preserved by the transformation;
- positive and negative sequence values of a purely sinusoidal signal are constant;

- positive and negative sequence values of a signal with even harmonic content are oscillating;
- zero sequence values of a signal with even harmonic content are zero;
- positive and negative sequence values of a signal with odd harmonic content are constant;
- zero sequence values of a signal with odd harmonic content are non-zero.

The use of the instantaneous phase voltage values to calculate the balanced voltages is demonstrated in the next figures. Figure 60 gives the moving average RMS values of the zero, positive and negative sequence components for a measured voltage dip which is almost symmetrical. Figure 61 gives the differences between the original measured instantaneous phase voltages and the reconstructed balanced phase voltages. Since the dip is almost symmetrical, the differences are only a few volts.

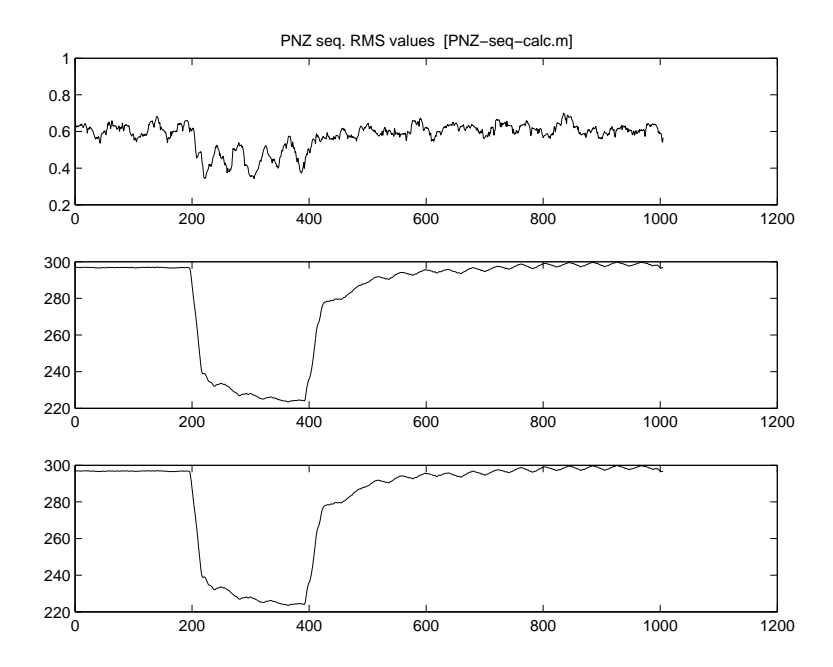


Figure 60: Moving average RMS values of the zero, positive and negative sequence for a symmetrical measured voltage dip

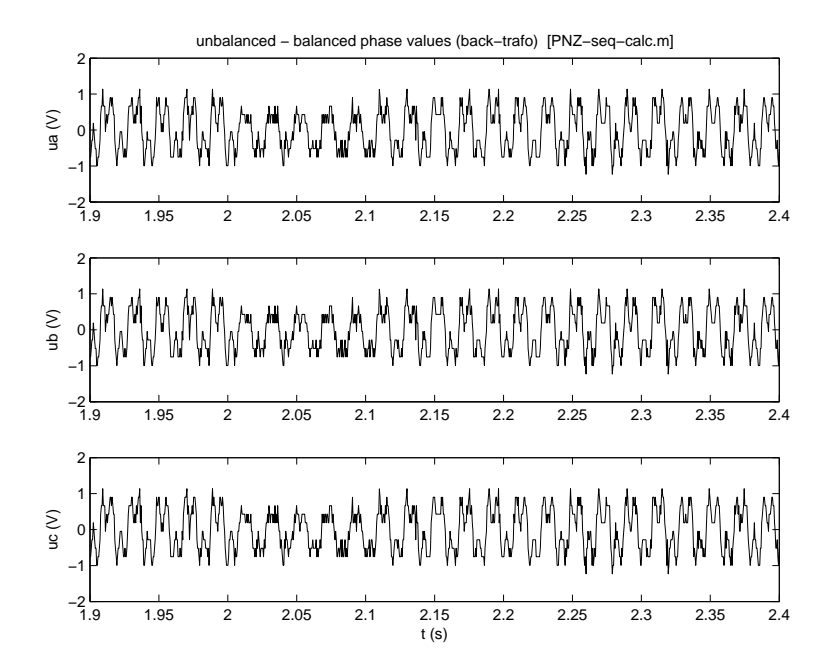


Figure 61: Differences between the original measured instantaneous phase voltages and the reconstructed balanced phase voltages

If  $v_a, v_b$  and  $v_c$  are the instantaneous phase voltages and  $i_a, i_b$  and  $i_c$  the instantaneous phase currents, the total instantaneous three phase power equals:

$$p = v_a i_a + v_b i_b + v_c i_c \tag{33}$$

Expressing the phase voltages and currents in terms of their symmetrical components, it can be shown that the total instantaneous three phase power equals [2]:

$$p = 3(v_{a0}i_{a0} + v_{a1}i_{a1} + v_{a2}i_{a2}) (34)$$

The first term is real, the second and third terms are complex conjugates and the sum is also real. Now if we want to eliminate asymmetrical aspects in a measurement, for instance a voltage dip, we can disregard the zero and negative sequence components calculated from the measurement.

The moving average RMS values can be calculated for a moving window of measured instantaneous values by adding the square of the instantaneous values, divide this value by the number of measurement samples and taking the square root of this value:

$$V_{rms} = \sqrt{\frac{\sum_{i=1}^{N} v_i \cdot v_i}{N}} \tag{35}$$

The moving average fundamental harmonic component of a phase quantity can be determined from a moving window of measured instantaneous phase values by calculating the fourier transform for this window. If the number of data points is relatively small, it is useful to interpolate the data first, for instance using a spline procedure.

# C SIMULATION PARAMETERS

The following list of the parameter values and labels of the VSP model input structures turb, wind, ctrg, ctrp, dcon, cmale and <math>simu have been prepared by plotstruct - JP.m.

Turbine parameters and labels:

```
turb.p.v
   .rotCfg
     .B 3
      .Rb 46
      .TqDdtmax4Pitch 120
      .TdelPtLoad 0.1
   .rotMod
      .LbTb 2
                     2.25
                                  2.5
      .ThTb -2 -1 0
                     0.0067689
      .CqTb 0.00562
                                   0.008664
      .CtTb 0.0949
                     0.10688
                                   0.12041
      .betapt 0.4
      .w0pt 80
      .Gpt1 1
      .Gpt2 0.95
      .Gpt3 1.05
   .rho 1.225
   .oprMod
      .Vwrat 12.3056
   .oprCfg
      .Vwcutout 25
   .dynfMod
      .pVwrTdTqPitch 0.00014542 -0.0093806
                                                 0.24562
      .pVwrTdFnPitch 9.5817e-005 -0.006176
                                                  0.17546
      .pVwrTi 9.8534e-005 -0.0063854
   .drvtrCfg
      .C1 0
      .C2 32000
      .iTran 70.65
      .Jr 12606000
      .Jg 1192900
   .drvtrMod
      .kdr 15748695.2237
      .cdr 910358128.0182
      .betags 0.4
      .w0gs 62.8319
   .towMod
      .kt 5821.4969
      .ct 1280214.0218
      .mt 264720
   .towCfg
      .Zt 94
turb.p.l
   .rotCfg
      .B Number of blades
      .Rb Rotor radius
      .TqDdtmax4Pitch Max. pitch trq gradient
      .TdelPtLoad Extra pitch delay spd rev
   .rotMod
      .LbTb Rough grid Lb-column
      .ThTb Rough grid Th-row
```

62 ECN-E-07-008

```
.CtTb Rough grid Ct-table
      .betapt Pitch damping rate
      .wOpt Pitch bandwidth
      .Gpt1 Pitch servo gain blade 1
      .Gpt2 Pitch servo gain blade 2
      .Gpt3 Pitch servo gain blade 3
   .rho Air density
   .oprMod
      .Vwrat Wind speed at which rated oper
   .oprCfg
      .Vwcutout Cut-out wind speed (10min)
   .dynfMod
      .pVwrTdTqPitch polyCf to Vw of 1/TauD for Tq
      .pVwrTdFnPitch polyCf to Vw of 1/TauD for Fa
      .pVwrTi polyCf to Vw of 1/TauI for Tq+
   .drvtrCfg
      .Cl Loss constant (Coulomb frictio
      .C2 Loss constant (viscous frictio
      .iTran Gearbox transmission ratio
      .Jr Moment of inertia turbine roto
      .Jg Moment of inertia generator ro
   .drvtrMod
      .kdr Drv. train eq. damping (1st mo
      .cdr Drv. train eq. stiffness (1st
      .betags E-torque servo system damping
      .w0gs E-torque servo system cut-off
   .towMod
      .kt Tower eq. damping (1st mode)
      .ct Tower eq. stiffness (1st mode)
      .mt Tower top eq. mass (1st mode)
   .towCfg
      .Zt Hub Height
Wind parameters and labels:
wind.p.v
   .windMod
      .TdelSimVw 0.1
      .VwMean 12.3056
      .UhubVw 12.3056
      .VwGrow4Adap2Mean 0.3
      .VwAmplGust 0
      .VwGrow4Gust 0.5
                            0.020628
      .nvwrotsmp0 0.01871
                                         0.024841
      .azimbase 0 0.16305 0.3261
      .nvwtow 0.012115 0.0098115 0.0084919
      .normazimbase 0 1 2
      .nvwshr -0.0024676 -0.0023437 -0.0022491
      .nvwrotsmp36 -0.032611 -0.025759 -0.0071924
      .ButtonWindSource 1
      .VwTbegGust 10
      .VwTdurGust 200
      .vwstair 9.99157
                           10.0047
                                        10.0478
wind.p.l
   .windMod
      .TdelSimVw Time step in generated wind sp
      .VwMean Mean wind speed during simulat
```

.CqTb Rough grid Cq-table

63

```
.UhubVw Wind speed ref. for wind speed
.VwGrow4Adap2Mean Initial wind speed growing rat
.VwAmplGust Wind gust amplitude
.VwGrow4Gust Wind gust growing rate
.nvwrotsmp0 Norm. Op rotor effective wind
.azimbase Azimuth base for wind speed se
.nvwtow Norm. wind speed variations by
.normazimbase Norm. azimuth base for azimuth
.nvwshr Norm. wind speed variations by
.nvwrotsmp36 Norm. 3p+6p rotor effective wi
.ButtonWindSource Type of windsource
.VwTbegGust Start time of wind gust
.VwTdurGust Duration of wind gust
.vwstair Staircase shaped wind speed se
```

#### Generator master controller parameters and labels:

```
ctrq.p.v
   .samplCfg
      .TdelCtrg 0.1
   .oprCfg
      .Pelrat 2750000
   .oprMod
      .NOptout 1.5049
      .Nrat 1.6305
      .TeOptout 486884.1346
      .pTe 213296.9817
                             4530.04946
                                            -2986.788315
      .NpTe 2
      .NPartin 1.0472
      .NOptin 1.0731
      .TeOptin 247342.968
   .button
      .BridgingOn 0
   .gcvDsgn
      .RpmDecrMax 1.5
      .dTmaxRate 200000
      .NskipRise 1.6232
      .NskipIn 1.6755
      .NskipOut 1.9687
      .NskipFall 1.5049
      .TskipRise 566326.1098
      .TskipIn 400000
      .TskipOut 140000
      .TskipFall 530000
   .gcvSyn
      .TBandIn 1737211.4694
      .RpmBandIn 14.663
      .RpmBandOut 16.5331
      .Phigh 2832500
      .Plow 2667500
      .WeightPfMnOld 0.99751
ctrg.p.l
   .samplCfg
      .TdelCtrg Cycle time for generator torqu
   .oprCfg
      .Pelrat Rated electric power
   .oprMod
      .NOptout End LbOpt generator angular fr
      .Nrat Rated angular generator speed
```

```
.TeOptout End LbOpt electric torque (SSE
   .pTe Polynomial coefficients Te=f(N
   .NpTe Poly degree of Te=f(Nr) for Lb
   .NPartin Gen. angular freq. production
   .NOptin Start LbOpt generator angular
   .TeOptin Start LbOpt electric torque (S
.button
  .BridgingOn Y/N Bridging tower resonance b
.gcvDsgn
  .RpmDecrMax Maximal transition shift below
  .dTmaxRate Maximum rate for electric torg
  .NskipRise Tow. res bridging, >NOptin
  .NskipIn Tow. res bridging, >NskipRise
  .NskipOut Tow. res bridging, >NskipIn
  .NskipFall Tow res bridging, >NskipOut an
  .TskipRise Tow res bridging
  .TskipIn Tow. res bridging, >TskipRise
  .TskipOut Tow. res bridging, <TskipIn an
   .TskipFall Tow. res bridging, >TskipOut a
.gcvSyn
  .TBandIn Min. elec. torque for gen. cha
   .RpmBandIn Min. rotor speed for gen. char
   .RpmBandOut Max. rotor speed for gen. char
   .Phigh Max. E-power for gen. char shi
   .Plow Min. E-power for gen. char shi
   .WeightPfMnOld Weighting factor for auto recu
```

#### Pitch control parameters and labels:

```
ctrp.p.v
   .samplCfg
     .TdelCtrp 0.1
   .oprCfg
     .RpmRat 15.57
   .but.ton
     .VwEst 1
      .EWFF 1
      .Fuz 1
      .DInf 1
   .drvtrCfg
      .C1 0
      .C2 32000
   .drvtrMod
     .Jeff 13798900
   .wseDsqn
     .VwWSE 6.9741
                       8.045
                                   9.4242
                              7.1111
     .ThWSE 0
                 3.5556
                                                1460582.4642
     .TaWSE 695515.45915
                             1078048.9617
     .NrWSE 1.5258
                        1.5886
                                    1.6514
   .ewffDsqn
     .VwEWFF 11.9802
                          12.2773
                                       12.5817
      .NrEWFF 1.5258
                         1.5886
                                     1.6514
      .dThdVwEWFF 4 4 4
   .ptune
     .NTdiffOld 0.83333
      .Gamma 0.5
      .RpmMintoVane 15.57
      .RpmMaxtoWork 16.57
      .ThULAdapNref 12
      .ThLLAdapNref 5
```

```
.NRefOld 0.9901
      .RpmRatOffMax 0
      .MuKsubnom 1
      .PercCtrl 1
      .ThIZPart 0.001
      .dThdtIZPart 0.25
      .dThdtIZFull 0.3
      .dThdtHysIZPart 0.25
      .dThdtHysIZFull 0.25
      .dThdtIZComp 0.25
      .dThdtIZVwSens 0.57685
      .ThDifSynchr 0.1
      .Ksynchr 1.52
      .NrpmWeighLPF 0.9901
      .NrpmForDrop 15
      .NrpmForLift 15.75
   .sfDsgn
      .SF2D 1
      .NrSF 14.57
                                     15.77
                       15.17
      .ThSF 0 1.4047 2.9097
      .GainSF 7 7 7
   .pdfbDsqn
      .PDxFac 1
      .PDsFac 0
      .KpNr -1.4002
      .KdNr -19.5791
   .pconstr
      .NrpmLimFuz 18.402
      .NrpmDdtLimFuz 0
      .dThdtFuzTarg 3
      .DeltaThFuz 3
      .ThErrmin4Strt 5
      .dThdtAllowStrt 1
      .ThAccLim2Vane 12.5
      .ThAccLim2Work -12.5
   .partCtrl
      .ThdgPartList 1 1 1
      .NrpmPartList 9.91
                               10.72
                                             11.53
      .Kpart 2.31
      .KpartxFac 0.8
   .diDsgn
      .pThrTdComp 5.0305e-006 0.00013999
                                             0.023127
      .pThrTiComp 8.9168e-006 -9.334e-005
                                             0.028808
      .NpTh 3
ctrp.p.l
   .samplCfg
      .TdelCtrp Cycle time for pitch control
   .oprCfg
      .RpmRat Rated generator speed (SSE)
   button
      .VwEst Y/N wind speed estimation
      .EWFF Y/N wind speed feed forward co
     .Fuz Y/N forced rotor speed limitat
      .DInf Y/N dynamic inflow compensatio
      .Cl Loss constant (Coulomb frictio
      .C2 Loss constant (viscous frictio
   .drvtrMod
      .Jeff Overall moment of inertia (SSE
```

```
.wseDsan
   .VwWSE Wind speed array for wind spee
   .ThWSE Pitch angle vector for wind sp
   .TaWSE Aero torque vector for wind sp
   .NrWSE Rotor speed vector for wind sp
.ewffDsqn
   .VwEWFF Wind speed vector for wind spe
   .NrEWFF Rotor speed vector for wind sp
   .dThdVwEWFF Scheduling gain array for wind
.ptune
  .NTdiffOld Weighting factor for different
   .Gamma Gain factor EWFF control
   .RpmMintoVane Rotor speed at which EWFF only
   .RpmMaxtoWork Rotor speed at which EWFF only
  .ThULAdapNref Upper pitch angle limit for ro
   .ThLLAdapNref Lower pitch angle limit for ro
   .NRefOld Weighting factor for rotor spe
   .RpmRatOffMax Maximum rotor speed setpoint i
   .MuKsubnom Extra control gain for rotor s
   .PercCtrl Extra overall full load contro
   .ThIZPart Pitch angle inactivity zone at
   .dThdtIZPart Pitch speed inactivity zone at
   .dThdtIZFull Inactivity zone at full load
   .dThdtHysIZPart Hysteresis factor at partial l
   .dThdtHysIZFull Hysteresis factor at full load
   .dThdtIZComp Extra gain at leaving or enter
   .dThdtIZVwSens IZ weakening factor for high t
   .ThDifSynchr Inactivity zone in blade pitch
   .Ksynchr Proportional gain blade pitch
   .NrpmWeighLPF Weighting factor for filter of
   .NrpmForDrop Lower rotor speed limit for pi
   .NrpmForLift Upper rotor speed limit for pi
.sfDsqn
   .SF2D 1D (Th) or 2D (Nr,Th) scheduli
   .NrSF Rotor speed vector for schedul
   .ThSF Pitch angle vector for schedul
   .GainSF Gain array for gain scheduling
.pdfbDsgn
   .PDxFac Extra PD control gain/weakenin
   .PDsFac Smooting factor D control
   .KpNr Proportional gain design value
   .KdNr Differential gain design value
.pconstr
   .NrpmLimFuz Rotor speed level at which for
   .NrpmDdtLimFuz Rotor acceleration at which fo
   .dThdtFuzTarg Pitch speed during forced roto
   .DeltaThFuz Pitch angle correction forced
   .ThErrmin4Strt Threshold pitch angle start-up
   .dThdtAllowStrt Allowed pitch speed start-up
   .ThAccLim2Vane Allowed pitch acceleration to
   .ThAccLim2Work Allowed pitch acceleration to
.partCtrl
   .ThdgPartList Pitch angle base points for pa
   .NrpmPartList Rotor speed base points for pa
   .Kpart Proportional gain of pitch ang
   .KpartxFac Extra control gain/weakening
   .pThrTdComp DIC PolyCf to Th of 1/TauDcomp
   .pThrTiComp DIC PolyCf to Th of 1/TauIcomp
   .NpTh Degree for non linear time con
```

#### Control mode parameters and labels:

```
cmod.p.v
   .samplCfg
      .TdelCmod 0.1
   .oprMod
      .Nrat 1.6305
      .NOptout 1.5049
      .NOptin 1.0731
      .NPartin 1.0472
      .TeOptout 486884.1346
   .ptune
      .RpmToFull 15.82
      .RpmToPartial 15.07
      .dTh2Part 0.5
   .pconstr
      .ThminPart 1
      .ThmaxPart 85
      .dThdtAllowPart 0.8
      .ThminFull 1
      .ThmaxFull 85
      .dThdtAllowFull 4
      .ThErrmin4Strt 5
      .ThminStrt 1
      .ThmaxStrt 85
      .dThdtAllowStrt 1
   .oprCfg
      .RpmRat 15.57
      .Pelrat 2750000
   .button
      .KarSft 1
   .gcvDsgn
      .PdeltaFac 0.03
      .RpmDecrMax 1.5
      .SftBack 0.1
cmod.p.1
   .samplCfg
      .TdelCmod Cycle time for control mode
   .oprMod
      .Nrat Rated angular generator speed
      .NOptout End LbOpt generator angular fr
      .NOptin Start LbOpt generator angular
      .NPartin Gen. angular freq. production
      .TeOptout End LbOpt electric torque (SSE
   .ptune
      .RpmToFull Rotor speed for switch partial
      .RpmToPartial Rotor speed for switch partial
      .dTh2Part Pitch angle diff. switch full
   .pconstr
      .ThminPart Minimum allowed pitch angle pa
      .ThmaxPart Maximum allowed pitch angle pa
      .dThdtAllowPart Allowed pitch speed partial lo
      .ThminFull Minimum allowed pitch angle fu
      .ThmaxFull Maximum allowed pitch angle fu
      .dThdtAllowFull Allowed pitch speed full load
      .ThErrmin4Strt Threshold pitch angle start-up
      .ThminStrt Minimum allowed pitch angle st
      .ThmaxStrt Maximum allowed pitch angle st
      .dThdtAllowStrt Allowed pitch speed start-up
   .oprCfg
```

```
.RpmRat Rated generator speed (SSE)
.Pelrat Rated electric power
.button
.KarSft Y/N Dynamic QN-curve shift
.gcvDsgn
.PdeltaFac Rel. max E-power overshoot for
.RpmDecrMax Maximal transition shift below
.SftBack Shift back rate for full/part-
```

#### Data conditioning parameters and labels:

```
dcon.p.v
   .samplCfg
      .TdelDcon 0.1
   .lopNrFilt
      .a 0.3788
                   0.32718
                              -0.19381
      .g -1.679e-016
                      1.2365 1.36e-015
      .b 0.40456
                 0.095999
                                0.46987
      .c -0.038547
                       0.3667 -0.021635
      .d 0.093453
   .bnt1NrFilt
      .a 0.76777
                    -0.25355
                               -0.57286
      .g -7.8224e-018 -8.3267e-017 4.1633e-017
      .b 0.065893
                    0.39623
                              -0.021353
      .c -0.41792
                    -0.53156
                                -0.13543
      .d 0.75311
      .k 1.122
   .bnt2NrFilt
      .a 0.97359
                  -0.078749
                               -0.21352
      .g -4.4434e-019 -2.2898e-016 8.6736e-017
      .b 0.0046862
                     0.11267 -0.00050699
      .c -0.57454
                     -0.6315 -0.062159
      .d 0.85367
      .k 1.122
   .button
      .Bnt1 1
      .Bnt2 1
dcon.p.l
   .samplCfg
      .TdelDcon Cycle time for data conditioni
   .lopNrFilt
      .a State transition matrix of LP
      .g Stationary gain vector from in
      .b Input vector of LP filter [Nx1
      .c Output vector of LP filter [1x
      .d Feedthrough scalar of LP filte
   .bnt1NrFilt
      .a State transition matrix of BNF
      .g Stationary gain vector from in
      .b Input vector of BNF1 filter [2
      .c Output vector of BNF1 filter [
      .d Feedthrough scalar of BNF1 fil
      .k Ripple compensation gain of BN
   .bnt2NrFilt
      .a State transition matrix of BNF
      .g Stationary gain vector from in
      .b Input vector of BNF2 filter [2
```

.c Output vector of BNF2 filter [

```
.d Feedthrough scalar of BNF2 fil
.k Ripple compensation gain of BN
.button
.Bnt1 Y/N band notch filter 1
.Bnt2 Y/N band notch filter 2
```

# Simulation parameters and labels:

```
simu.p.v

.simuCfg
    .TdurSim 300
    .TdelAcq 0.1

simu.p.l

.simuCfg
    .TdurSim Time duration of simulation
    .TdelAcq Sampling interval for data aqu
```